A degradable mode I cohesive zone model developed for damage and fracture analysis of dissimilar composite/metal adhesive joints subjected to cyclic ageing conditions

Moazzami, M.; Akhavan-Safar, A.; Ayatollahi, M. R.; Poulis, J. A.; da Silva, L. F.M.; Teixeira De Freitas, S.

DOI
10.1016/j.tafmec.2023.104076

Publication date
2023

Document Version
Final published version

Published in
Theoretical and Applied Fracture Mechanics

Theoretical and Applied Fracture Mechanics 127 (2023) 104076

Contents lists available at ScienceDirect

Theoretical and Applied Fracture Mechanics

journal homepage: www.elsevier.com/locate/tafmec

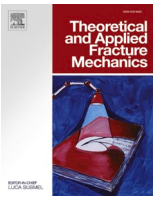

A degradable mode I cohesive zone model developed for damage and fracture analysis of dissimilar composite/metal adhesive joints subjected to cyclic ageing conditions

M. Moazzami [a], A. Akhavan-Safar [b], M.R. Ayatollahi [a], J.A. Poulis [c], L.F.M. da Silva [d], S. Teixeira De Freitas [c,*]

[a] Fatigue and Fracture Research Laboratory, Center of Excellence in Experimental Solid Mechanics and Dynamics, School of Mechanical Engineering, Iran University of Science and Technology, Tehran, Iran
[b] Institute of Science and Innovation in Mechanical and Industrial Engineering (INEGI), Porto, Portugal
[c] Structural Integrity Group, Faculty of Aerospace Engineering, Delft University of Technology, Delft, The Netherlands
[d] Department of Mechanical Engineering, Faculty of Engineering, University of Porto, Porto, Portugal

ARTICLE INFO

Keywords:
Cohesive zone modelling
Dissimilar adhesive joints
Cyclic ageing
Moisture diffusion
Mode I

ABSTRACT

Adhesive joints are frequently exposed to cyclic ageing conditions during their service life, which can have a substantial impact on the mechanical properties of both the adhesive and the substrates. The safe life philosophy, commonly employed in the design of bonded joints, underscores the importance of obtaining an accurate estimate of the adhesive's durability. Therefore, it is essential to enhance the predictive capabilities of the adhesive's mechanical behavior under cyclic ageing conditions.

This research aims to expand the use of quasi-static cohesive zone modelling (CZM) for damage and fracture analysis of dissimilar adhesive joints subjected to cyclic ageing environments. The first step involved measuring the mechanical properties of the adhesive through tensile tests on unaged and cyclically aged dogbone specimens, considering their moisture content and ageing cycles. Based on the results, a degradable CZM was developed. To validate the numerical model, dissimilar double cantilever beam specimens (DCBs) of glass fibre reinforced polymer (GFRP) and aluminium were manufactured and tested before and after ageing. The load-displacement curves of the bi-materials bonded joints were successfully predicted using the developed model where the properties of the material are defined as a function of the moisture uptake and ageing cycles at each material element. The obtained results showed that after 4 ageing cycles, the maximum load of DCB specimens decrease considerably.

1. Introduction

Adhesion technology is widely utilized in various industries, including aeronautics and automotive, as it offers several advantages over traditional bonding methods such as riveting and bolting. These conventional methods can lead to pre-damage of the substrates, while welding cannot bond dissimilar materials like composites and metals. Adhesion technology provides a solution to these limitations [1]. In recent years, glass fibre reinforced polymer (GFRP) composites have gained significant attention and utilization because of their outstanding mechanical properties and cost-effectiveness [2]. For composite materials, adhesive bonding is one of the most common and suitable techniques used for joining [3,4]. This joining technique has been also considered for dissimilar joints where a GFRP substrate is bonded to a metal part using structural adhesives [1,5]. When designing dissimilar adhesive joints, the fracture energy plays a crucial role in determining their ability to withstand mechanical loads. Although the fracture energy of the joint is typically viewed as a material property, studies by various authors have demonstrated that it is also affected by the joint geometry. Hence, joint geometry should be taken into account when considering fracture energy in the design of dissimilar adhesive joints subjected to mechanical loads [6,7]. Accordingly, it is recommended to perform a dissimilar fracture test for joints that use dissimilar substrates.

The double cantilever beam (DCB) joint is a commonly used joint

* Corresponding author.
E-mail address: S.TeixeiraDeFreitas@tudelft.nl (S. Teixeira De Freitas).

https://doi.org/10.1016/j.tafmec.2023.104076
Received 12 May 2023; Received in revised form 3 August 2023; Accepted 1 September 2023
Available online 3 September 2023

Table 1
Mechanical properties of material used in this study (direction 1 is along the fibre (longitudinal); and 2 denotes the transverse direction).

Material	E_1(MPa)	E_2(MPa)	G_{12}(MPa)	ϑ_{12}	$G_{1c}(J/m^2)$
UD-0° E-glass lamina [8]	38,070	11,160	3951	0.28	–
Aluminium 7076-T6 [22]	71,000 ±3500	–	–	0.33	–
Araldite 2011 [22]	1550 ±150	–	–	0.45	2116

geometry for fracture analysis of adhesive joints. In DCB specimens with the same substrates, mode I fracture energy can be studied effectively. However, achieving mode I condition in dissimilar DCB adhesive joints is a challenge. To address this issue, previous studies have proposed various approach for mode I loading in DCB joints made by dissimilar substrates.

One approach proposed by researchers is to design the joint based on an equivalent bending (flexural) stiffness of the substrates used in the DCB joint. Using an equivalent longitudinal strain distribution at the interface has been also proposed by some authors to achieve mode I condition in DCBs with dissimilar substrates [8–10]. It is asserted by Wang et al. [8] that the latter technique is more effective as its results is closer to pure mode I. In summary, selecting an appropriate loading technique is critical in achieving mode I condition in DCBs with non-similar substrates. The choice of loading technique depends on various factors, such as the substrate materials, joint geometry, and experimental conditions.

Adhesive joints in applications such as airplane and marine structures[2,11] often experience high humidity conditions, which can affect their mechanical properties [12–14]. Moisture diffusion can alter the Young's modulus and tensile strength of adhesives, reducing the former and the latter and increasing their ductility [15–19]. Previous studies have shown that moisture diffusion can increase or in some cases decrease the fracture energy of adhesives, depending on the dominant moisture diffusion mechanisms in the adhesive [20–23]. For example, Fernandes et al. [20] found that the fracture energy of adhesives changes depending on the ageing conditions, with distilled water reducing the fracture energy and a saltwater environment increasing it. In contrast, some authors [24] analyzed the residual strength of single lap joints exposed to ageing and found that the adhesive joints strength initially decreases during the first 20 days but then increases by 40 days. These contradicting results suggest that understanding the mechanisms of moisture diffusion and their effects on the mechanical properties of the joint is critical for designing adhesive joints that can withstand high

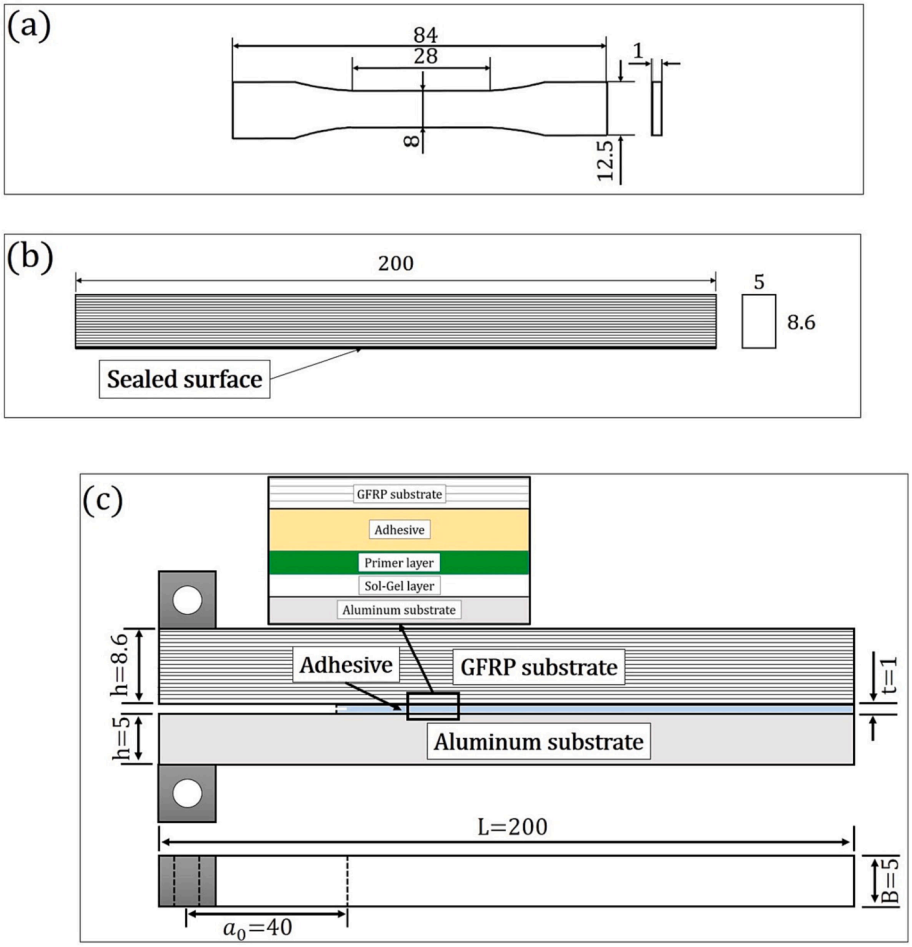

Fig. 1. Geometries of dogbone specimen (a), GFRP laminates (b), and DCB (c) (dimensions in mm and not to scale).

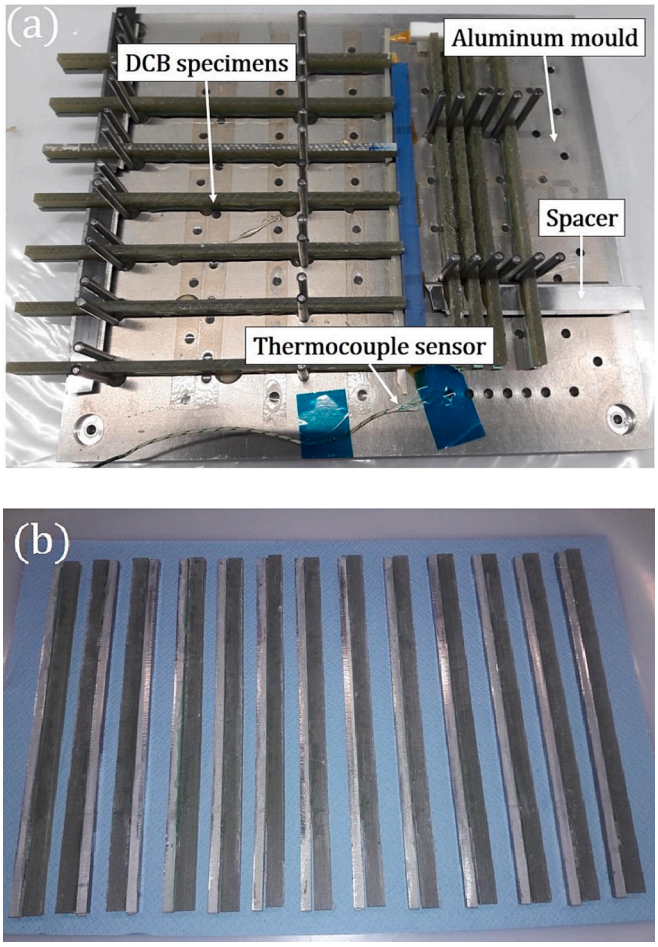

Fig. 2. DCB specimens: (a) in aluminium mould and (b) after curing.

humidity environments. Further research is needed to develop a more comprehensive understanding of the effects of moisture diffusion on adhesive joint performance and to develop effective strategies for mitigating these effects.

Moisture diffusion in composite substrates occurs through voids or micro cracks, as well as through the fibre/matrix interface via capillarity diffusion [25–27]. Two mechanisms have been proposed to explain the effects of moisture diffusion in composite structures: polymer plasticization and degradation of the fibre/matrix interface [28]. Experimental results have shown that moisture diffusion can significantly affect the fibre/matrix interface [29,30]. Moisture diffusion through the resin causes a volume expansion, while the fibre is non-absorbent [31]. This resin swelling creates residual stresses and can lead to debonding at the fibre/matrix interface [32]. It is important to note that the effects of moisture diffusion on composite structures depend on various factors, such as the type of composite material, environmental conditions, and duration of exposure. Therefore, understanding the specific mechanisms and effects of moisture diffusion on composite substrates is critical for designing and selecting materials that can withstand high humidity environments.

Moisture can be absorbed both monotonously and cyclically, while in many applications, adhesives are subjected to cyclic humidity [33–36]. According to a study conducted on the residual strength joints after different ageing times [37], it was revealed that moisture absorption and desorption results in degradation and recovery of the joint strength, respectively. Other authors [17,38] have also investigated the cyclic ageing of bulk adhesives and found that the Young's modulus of the adhesive degrade and recover during moisture absorption and desorption, respectively (the same results for the joint strength). Despite significant research on the effect of monotonous moisture uptake on adhesive joints in recent years, there is still limited understanding of the cyclic ageing effects on bonded joints, particularly those involving polymer composite substrates.

In this paper, the effect of cyclic ageing on the mechanical response of dissimilar DCB adhesive joints with GFRP/aluminium substrates is investigated. The aim of this research is to extend the quasi static cohesive zone modelling (CZM) technique for the damage and fracture analysis of dissimilar adhesive joints subjected to cyclic ageing environments.

2. Experimental procedure

2.1. Materials

In this study, three different types of specimens were manufactured: bulk dogbone, glass fiber reinforced polymer (GFRP) beams, and dissimilar DCB adhesive joints with aluminum-GFRP substrates. Araldite 2011 (Huntsman, Basel, Switzerland) that is an epoxy adhesive, was used to bond the substrates. To produce the bulk dogbone specimens, the two adhesive components were mixed using a SpeedMixer DAC 150^{TM} (Hauschild, Hamm, Germany) at 2300 rpm for 2 min. After mixing, the adhesive was cured between two glass plates to form adhesive sheets. To control the adhesive thickness, spacers with the thickness of 1 mm was used. The adhesive sheets were cured for 40 min at 80 °C according to the manufacturer's technical data sheet. The dog-bone bulk specimens were then cut from the cured adhesive sheets. The GFRP specimens were fabricated by layering four quadraxial E-glass layers, which consisted of unidirectional (UD) fabric oriented in the [45/90/+45/0] direction. This laminate was created through a vacuum infusion process. The GFRP laminate was cured at 23 °C for one day, and post cured at 60 °C 12 h [39]. GFRP and aluminum alloy 7075-T6 were bonded together to create the dissimilar joint. The properties of the materials used are listed in Table 1 [8,22].

2.2. Samples geometries

Dogbone specimens were created from bulk adhesive sheets to assess the elastic modulus and tensile strength of the adhesive under varying moisture diffusion conditions. Additionally, 12 GFRP specimens were tested to determine the flexural properties of the GFRP substrates in dissimilar double cantilever beam (DCB) adhesive joints during different ageing cycles. To simulate moisture diffusion boundary conditions of aged DCB adhesive joints on GFRP substrates, one side of the GFRP laminates was sealed with aluminum foil to prevent moisture absorption [40]. The GFRP substrates were then cyclically aged and tested after moisture absorption in various ageing cycles under three-point bending conditions. Dissimilar DCB specimens with GFRP/aluminum substrates were also fabricated, cyclically aged, and tested to obtain load–displacement curves in different ageing cycles. Fig. 1 provides a schematic representation of the dogbone, GFRP laminate, and dissimilar DCB adhesive joint geometries.

In order to speed up the effects of moisture diffusion on the dogbone and DCB specimens, a study by Costa et al. [41] suggested the use of mini dogbone and mini DCB specimens as shown in Fig. 1. The researchers found that there was a negligible difference in mechanical properties using the standard specimens and the mini specimen. Therefore, to accelerate the ageing process, dogbone and DCB specimens

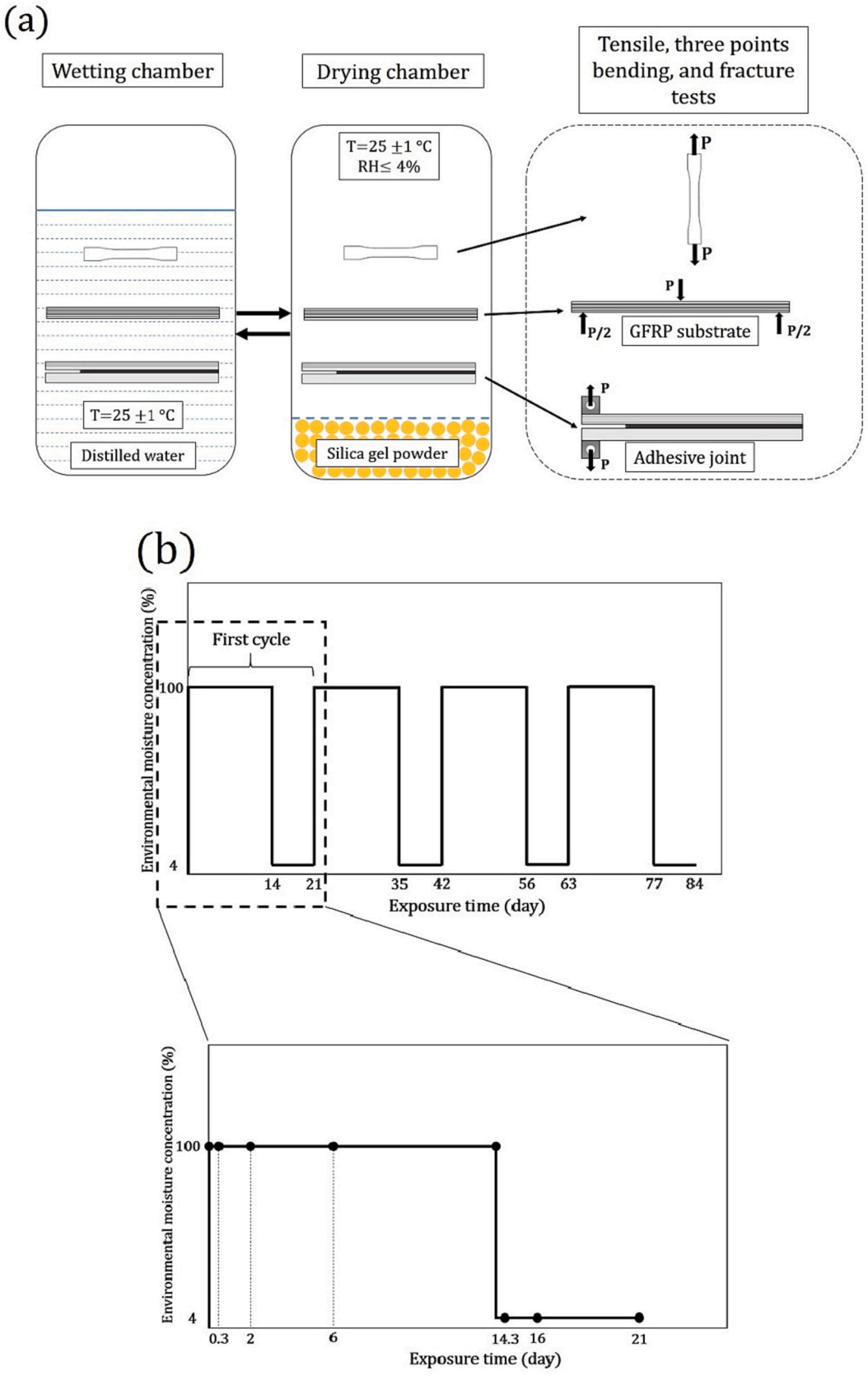

Fig. 3. The ageing conditions (a), and exposure times for dogbone samples (b).

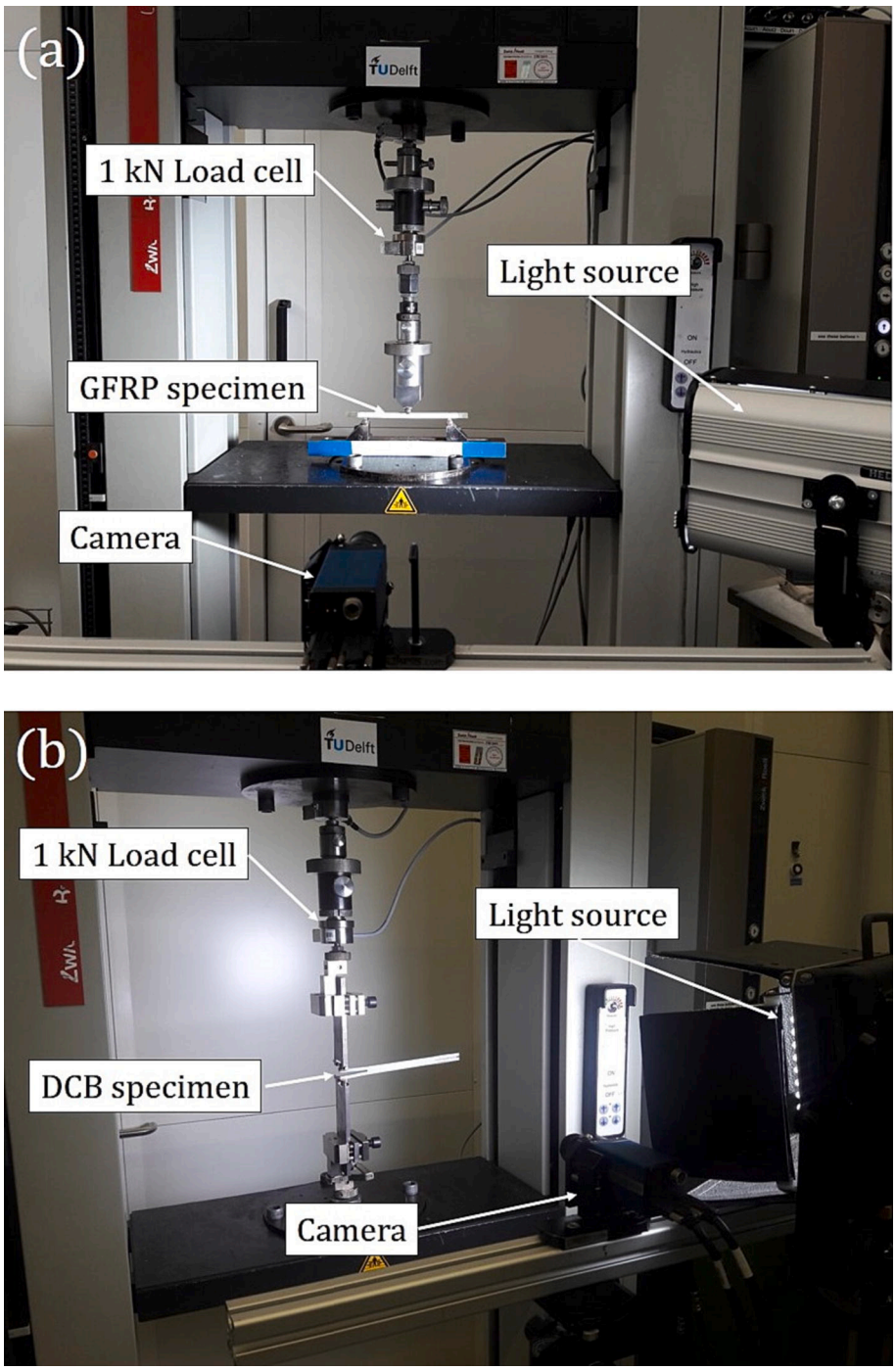

Fig. 4. Three points bending (a) and fracture (b) test setup.

were fabricated based on the previous findings [41]. The composite laminate was cut into the dimensions of 5 mm by 200 mm based on the geometry of mini DCBs, which are suitable for investigating ageing effects. To obtain a pure mode I condition, the longitudinal strain criterion was considered [8]. It should be noted that the thickness tolerances were 0.2 mm for the GFRP and 0.05 mm for the aluminium.

2.3. Manufacturing of DCBs

Several procedures were implemented to prepare the surfaces of substrates for bonding in the production of dissimilar double cantilever beam (DCB) adhesive joints. To begin with, the surface of GFRPs were sanded with sandpaper (240 grit) followed by acetone cleaning. The aluminium substrates, on the other hand, were grit blasted. Aluminium surfaces were then cleaned using acetone. The procedure was followed by immersing the aluminium specimens in a sol–gel AC-130 bath. The

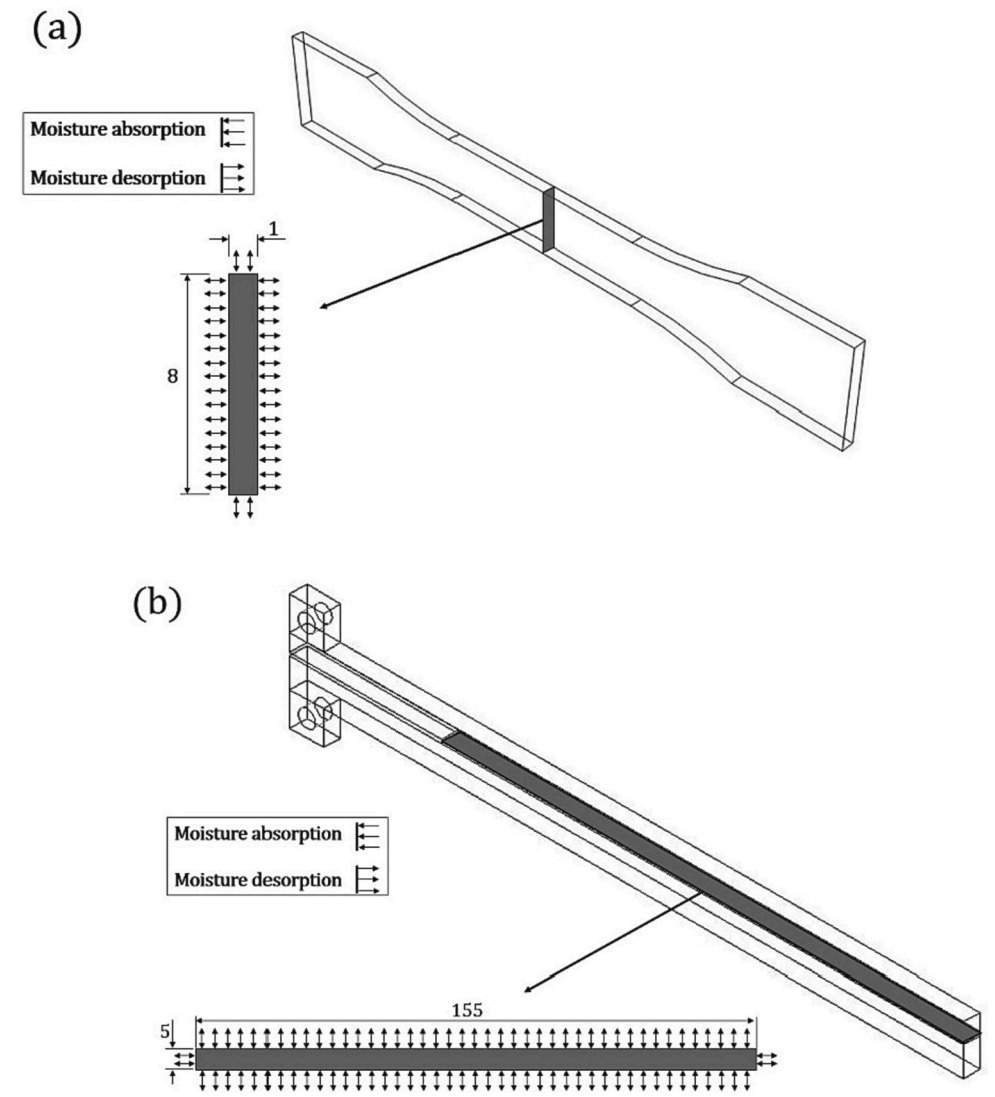

Fig. 5. Boundary conditions for dogbone samples (a) and DCB adhesive layer (b) (dimensions in mm).

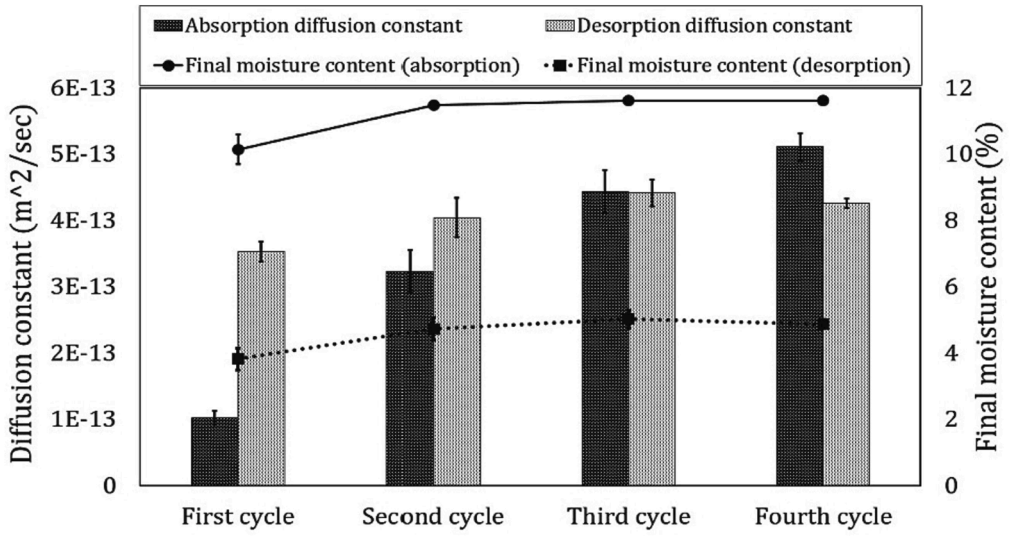

Fig. 6. Diffusion coefficients and final moisture contents in different absorption and desorption steps for Araldite 2011 [22].

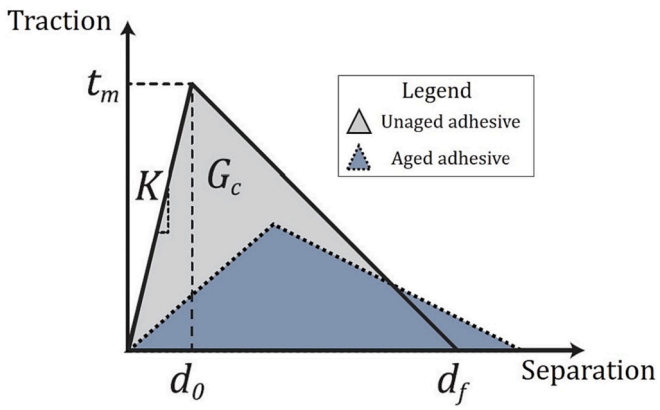

Fig. 7. Triangular traction-separation curves for unaged and aged adhesive.

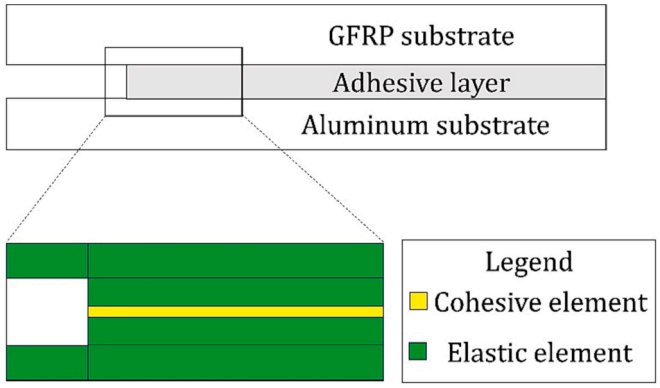

Fig. 8. Schematic of the configuration of the elastic and cohesive elements.

specimens were kept in the bath for 90 s following by 60 min drying at room temperature. To decrease moisture diffusion in the aluminium/adhesive interface and prevent interface failure after ageing, EW-5005 (that is a primer) was sprayed on the aluminium substrate surfaces. After 30 min keeping the samples at room temperature the primer was cured for 60 min by putting the samples in an oven set to 121 °C. Subsequently, Araldite 2011 was applied to the joints and then the DCBs were cured at 80 °C for 40 min. A pre-crack was made in the adhesive layer using a sharp razor blade during the fabrication, and an aluminium mould with spacers was used.

2.4. Ageing process

All of the produced specimens, including bulk dogbone, GFRP, and DCB adhesive joints, were subjected to 4 distinct ageing cycles, with each cycle consisting of 14 days of wetting followed by 7 days of drying. The cumulative duration of the ageing process was $(14 + 7) \times 4 = 84$ days, which is the product of the number of cycles and the total number of days for each cycle. The temperature of the ageing chamber was maintained at 25 ± 1 °C during both the wetting and drying stages. During wetting, the specimens were submerged in distilled water, whereas during drying, they were placed in a container containing silica gel powder with a relative humidity of less than 4 % (as shown in Fig. 3a).

The study selected and evaluated GFRP substrates and DCB adhesive joints after completing the absorption process in the 1st, 2^{ed}, and 4th ageing cycles. Dogbone samples were extracted from the ageing chamber at varying exposure durations and subjected to tensile loading. Fig. 3b illustrates the exposure durations during each cycle when the tensile tests of the dogbone specimens were carried out. The tensile tests of the aged dogbone samples were conducted at the same exposure durations in the 1st, 2^{ed}, and 4th cycles.

2.5. Experimental tests

During this research, three different types of experimental tests were conducted, including tensile tests, three-point bending tests, and mode I fracture tests. Tensile tests were performed at 23 °C and 35 % RH (relative humidity). To minimize experimental errors, each condition was tested three times. The loading rate was constant during the tensile tests and was set to 0.5 mm/min, and the crack length was recorded using a digital camera during fracture tests. Loading rate for dogbone

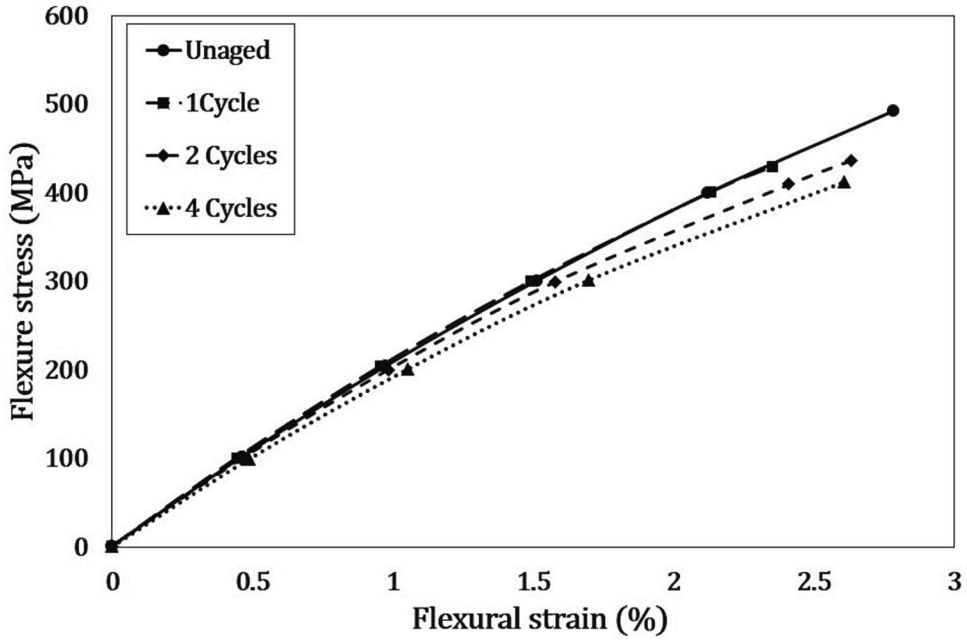

Fig. 9. Flexural stress–strain as a function of ageing cycles curves for GFRP substrates.

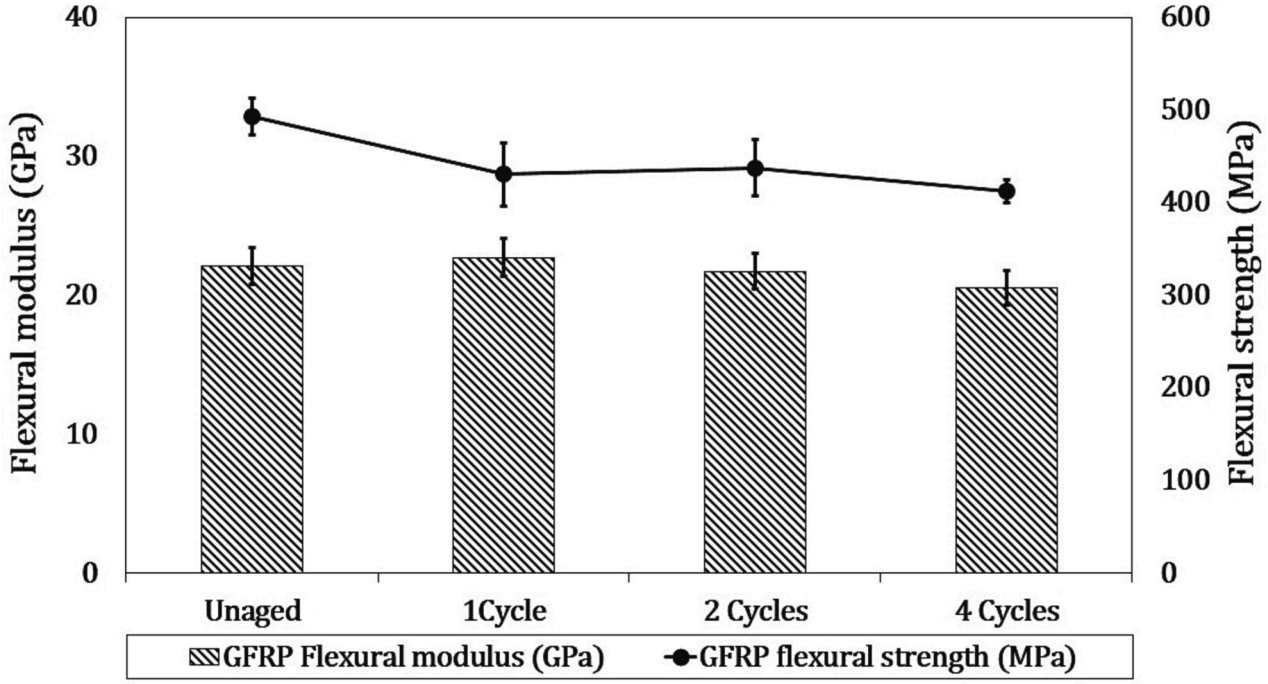

Fig. 10. Flexural modulus and strength of GFRP substrates for different numbers of ageing cycles.

and GFRP samples was considered as 1 mm/min, and the deformation of GFRP specimens and strains of the dogbone specimens were calculated using digital image correlation (DIC) data. Digital camera pictures were captured continuously from the specimen's (GFRP and dogbone) surface with a constant rate of one picture every second. The DIC setup consisted of an 8-bit "Point Grey'' camera with a resolution of 5 MP, equipped with a "XENOPLAN 1.4/23″ lens. The software used for capturing the images was VIC-Snap 8, a product of "Correlated Solutions Inc.". Using this setup, the resolution of the captured images was about 2048 × 2048 pixels. The output from the tensile test machine was used to synchronize the captured images with their corresponding load and displacement at different measurement times. The DIC setup was installed at a distance of 65 cm from the specimen surface. During the image correlation process the subset size and step size parameters were considered 51*51 and 7, respectively. The experimental setup for the fracture (DCB) and three-point bending (GFRP) tests is illustrated in Fig. 4.

During this investigation the crack propagation path through the adhesive layer was checked by a 3D measurement system (Keyence VR-3200 Wide-Area). In this process based on the height of substrate surface and fracture surface the thickness of remained adhesive on fractured substrates can be determined.

3. Numerical simulation

This research involved conducting numerical simulations in two stages. Firstly, the moisture distribution of the dogbone and adhesive layer of the DCB specimens were simulated for various ageing conditions. Secondly, based on the mechanical properties of the adhesive, which vary with moisture content and ageing cycles, load–displacement curves of DCB specimens were simulated using a degradable cohesive zone model.

3.1. Moisture diffusion simulation

To simulate the distribution of moisture in the dogbone specimens and in joints for different ageing conditions, FEM was employed. For this purpose the moisture diffusion constant and the final moisture contents were defined as the properties of absorbing material and boundary conditions, respectively. These parameters were obtained from a previous research performed by the authors and described in [22]. In that research, gravimetrical specimens were fabricated and exposed to cyclic aging. During the cyclic aging the gravimetrical specimens were weighed using electronic analytical balance with a precision of 0.1 mg continuously. Based on these results the moisture uptake of gravimetrical specimens in each aging cycle were obtained. In the simulation performed in the current paper, the moisture content of the specimen at the end of the aging cycles (final moisture content) is defined as the boundary conditions in the simulations. In addition, the diffusion constant in absorption and desorption process, were calculated from the initial slope of the moisture uptake versus time curve where this curve is linear using the Fick's law equation. In the current paper, this parameter is defined as the material properties in each aging cycles in FEM simulation. More details can be found in [22]. In this research the moisture diffusion constant and the final moisture contents (at the end of each ageing cycle) obtained in [22] were defined as the material properties and boundary conditions, respectively. Since there is some remaining moisture from the previous ageing cycles in cyclic ageing simulations, the final moisture distribution of each cycle was defined as the initial moisture distribution in the next cycle [22]. Abaqus software was used for the numerical simulation, utilizing eight-node quadratic heat transfer or DC2D8 (mass diffusion quadrilateral brick) elements. In total, 12,500 and 25,700 elements were used for the DCB adhesive layer and dogbone specimens, respectively. Fig. 5 illustrates the geometry of the boundary conditions for moisture for different specimens.

To simulate the moisture distribution in the adhesive layer, it is necessary to determine Fick's law constants as a function of ageing

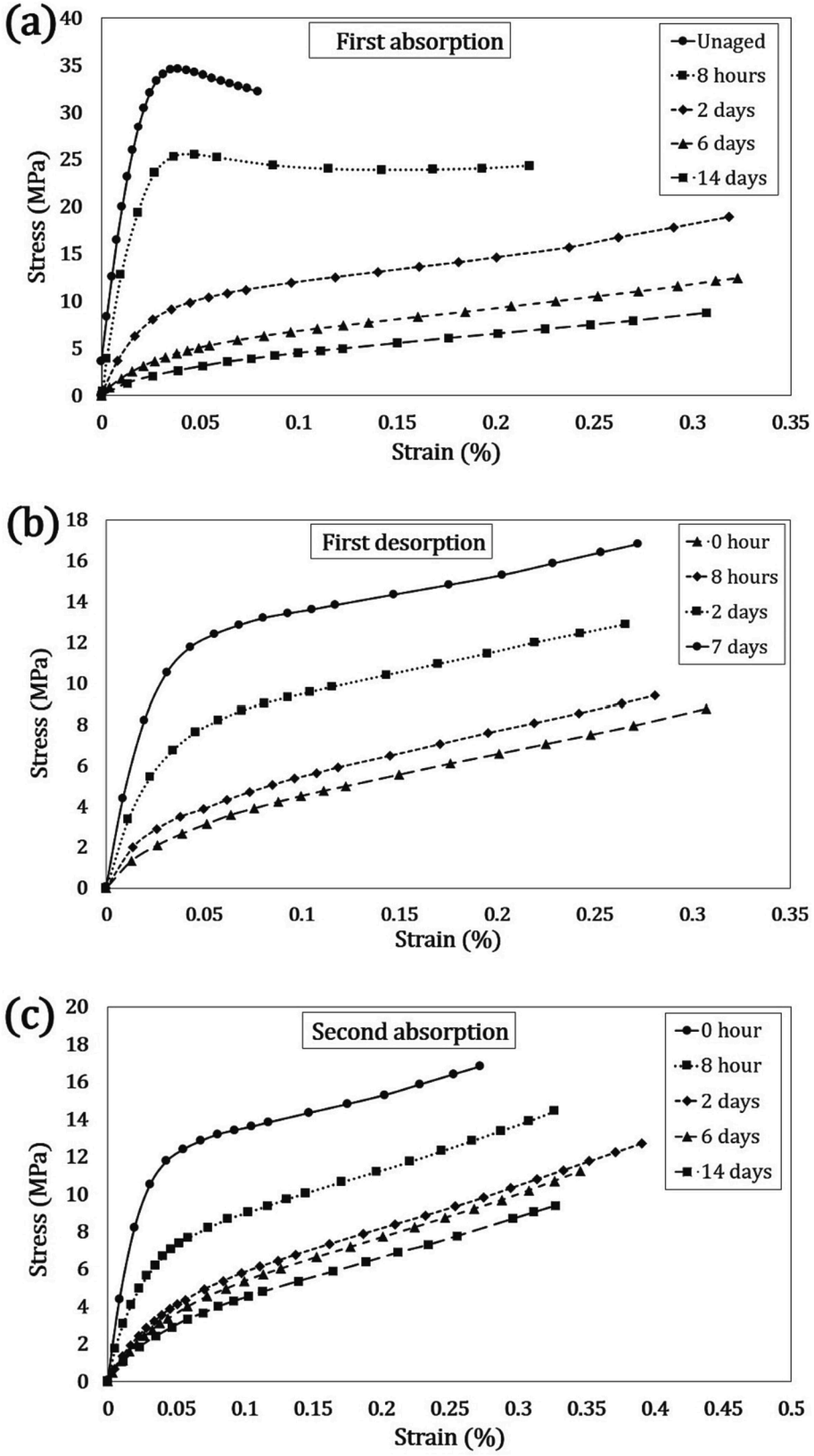

Fig. 11. Stress–strain curves for different ageing cycles and for both ageing and drying processes: (a) and (b) are for the first cycle (absorption and desorption, respectively), (c) and (d) are for the second cycle (absorption and desorption, respectively), and (e) and (f) are for the fourth cycle (absorption and desorption, respectively).

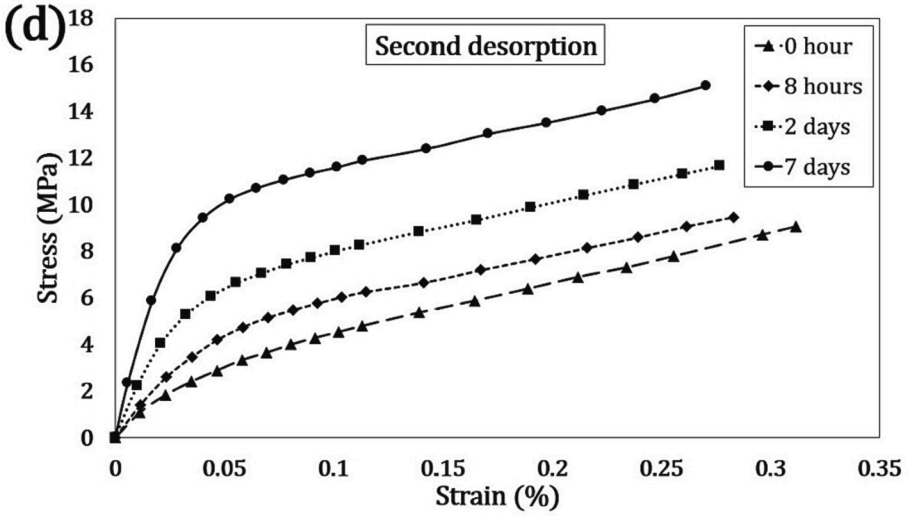

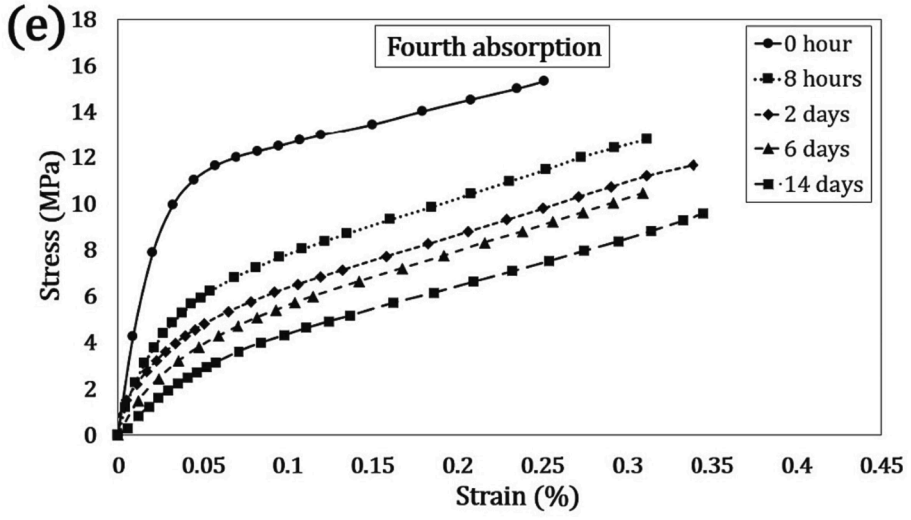

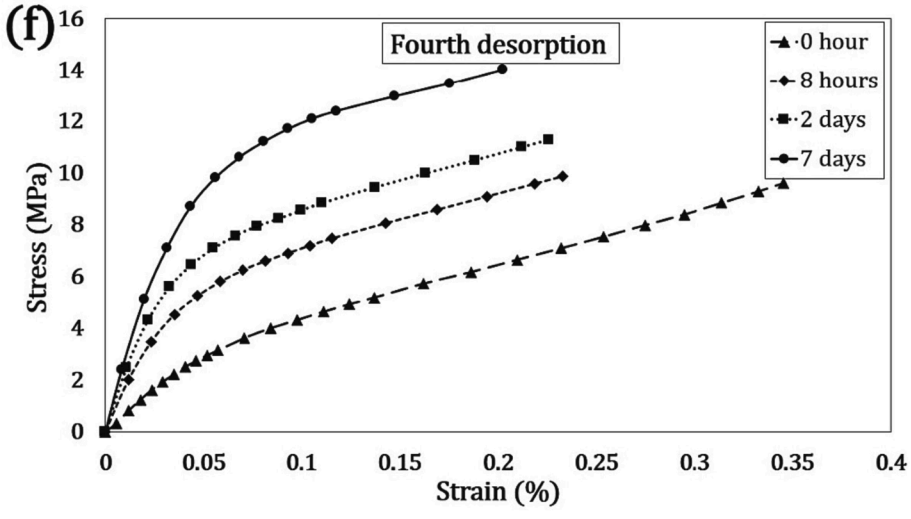

Fig. 11. (*continued*).

cycles. For Araldite 2011, the diffusion constant and moisture content at the end of ageing cycles were calculated in previous research [22]. Fig. 6 shows the Fick's law parameters for Araldite 2011.

3.2. Developing a degradable CZM as a function of ageing level/cycles

In this step, a numerical model based on a degradable cohesive zone approach was developed to estimate the load–displacement behavior of DCB specimens for different moisture contents and ageing cycles. The model was able to simulate the elastic region, damage initiation and evolution of the adhesive layer. The traction-separation law was used to relate the stress to the relative displacement of the nodes in the cohesive elements. Various curves were considered for the traction-separation law, but the model showed that the elastic deformation of the cohesive element was followed by a peak value of traction, after which the damage initiated, leading to complete failure of the adhesive layer. The developed model was validated by comparing its predictions with the experimental results [42,43]. The area under traction-separation curves represents the fracture energy of the adhesive. The most common types of traction-separation laws are triangular, exponential and trapezoidal [42,44,45]. In general, the triangular shapes are mostly suitable for brittle adhesives [46]. The trapezoidal curves consider plastic deformations and are used for ductile materials [47]. In this research, triangular traction-separation law was applied for Araldite 2011 (see Fig. 7).

Fig. 7 displays the triangular traction-separation curve, which is characterized by three primary parameters: initial stiffness, cohesive traction, and fracture energy. The initial stiffness (K in Fig. 7) and cohesive traction were determined by conducting tensile tests on bulk dogbone specimens, whereas the fracture energy was calculated in a prior study [22]. The initial stiffness was defined as $K = E/h_a$, where E represents the elastic modulus of the adhesive and h_a denotes the thickness of the adhesive layer. To determine the elastic modulus, the bulk adhesive dogbone specimens were subjected to cyclic ageing and tested under tensile conditions. The stress–strain curves obtained under different ageing conditions were used to calculate the elastic modulus and initial stiffness in CZM as a function of ageing level/cycles. The cohesive traction (t_m in Fig. 7) was established as the tensile strength of bulk dogbone specimens obtained from tensile tests of cyclically aged specimens. The mode I fracture energy, another crucial parameter in CZM, was measured using the open-DCB (ODCB) technique under varying moisture contents and ageing cycles [22]. The ODCB method was employed to accelerate moisture diffusion in the adhesive layer of DCB samples since the geometry of the normal DCB adhesive joint makes the moisture diffusion process time-consuming. CZM parameters change with different ageing conditions as a function of moisture content and ageing cycles and must be updated based on moisture diffusion conditions in each cohesive element. To achieve this, moisture concentration was simulated in the adhesive layer at the end of the moisture absorption process. Subsequently, a subroutine code was utilized to define the required cohesive parameters (initial stiffness, cohesive traction, and mode I fracture energy) of the adhesive in each element as a function of moisture contents and ageing cycles based on the simulated moisture content.

Within the Cohesive Zone Model (CZM), there are several methods that can be utilized for predicting the point of damage initiation (including maximum or quadratic values of the nominal or principal stress or strain), as well as for damage propagation (such as displacement or energy controlled). For the purposes of this study, a quadratic nominal stress approach was employed to determine the damage initiation, as demonstrated in Equation (1):

$$\left(\frac{t_n}{t_n^0}\right)^2 + \left(\frac{t_s}{t_s^0}\right)^2 = 1 \tag{1}$$

where, t_n is the tensile stress and t_s is the shear stress, respectively. t_n^0 and t_s^0 are the initiation tensile and shear stresses, respectively. It is further assumed that normal compressive stresses don't cause damage [48]. When the damage initiation equation is fulfilled, the softening of the material's stiffness starts. In this research, the damage evaluation process was controlled by the linear mode-mixity fracture energetic criterion, which is shown in Equation (2):

$$\frac{G_n}{G_n^C} + \frac{G_s}{G_s^c} = 1 \tag{2}$$

where, G_n is the normal energy and G_s is the shear energy. G_n^C in Equation (2) is the fracture energy in mode I and G_s^c is the fracture

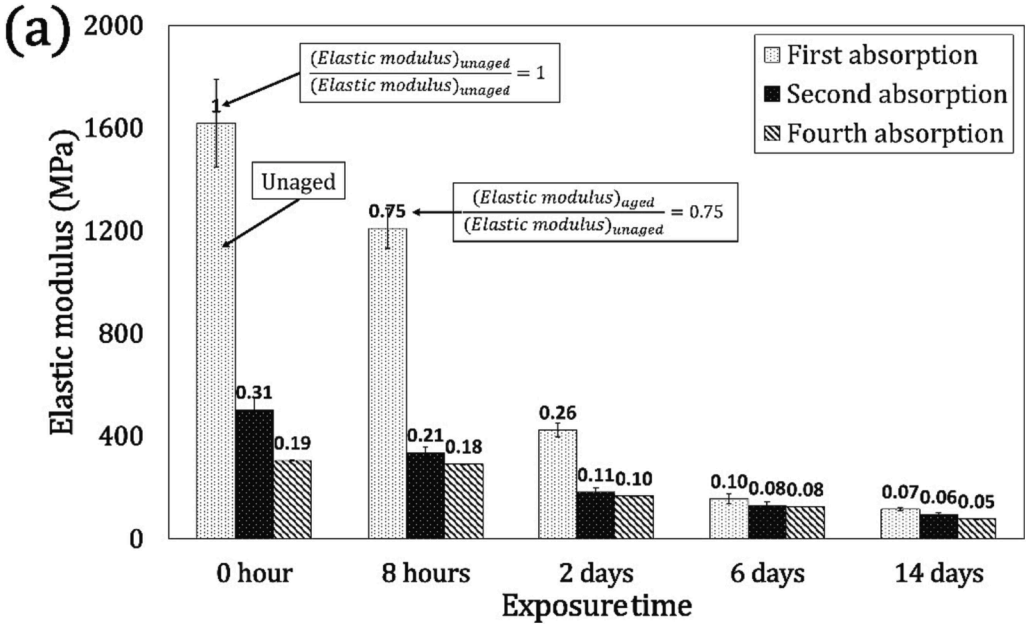

Fig. 12. Variation of elastic modulus during the (a) absorption and (b) desorption and tensile strength in (c) absorption and (d) desorption process.

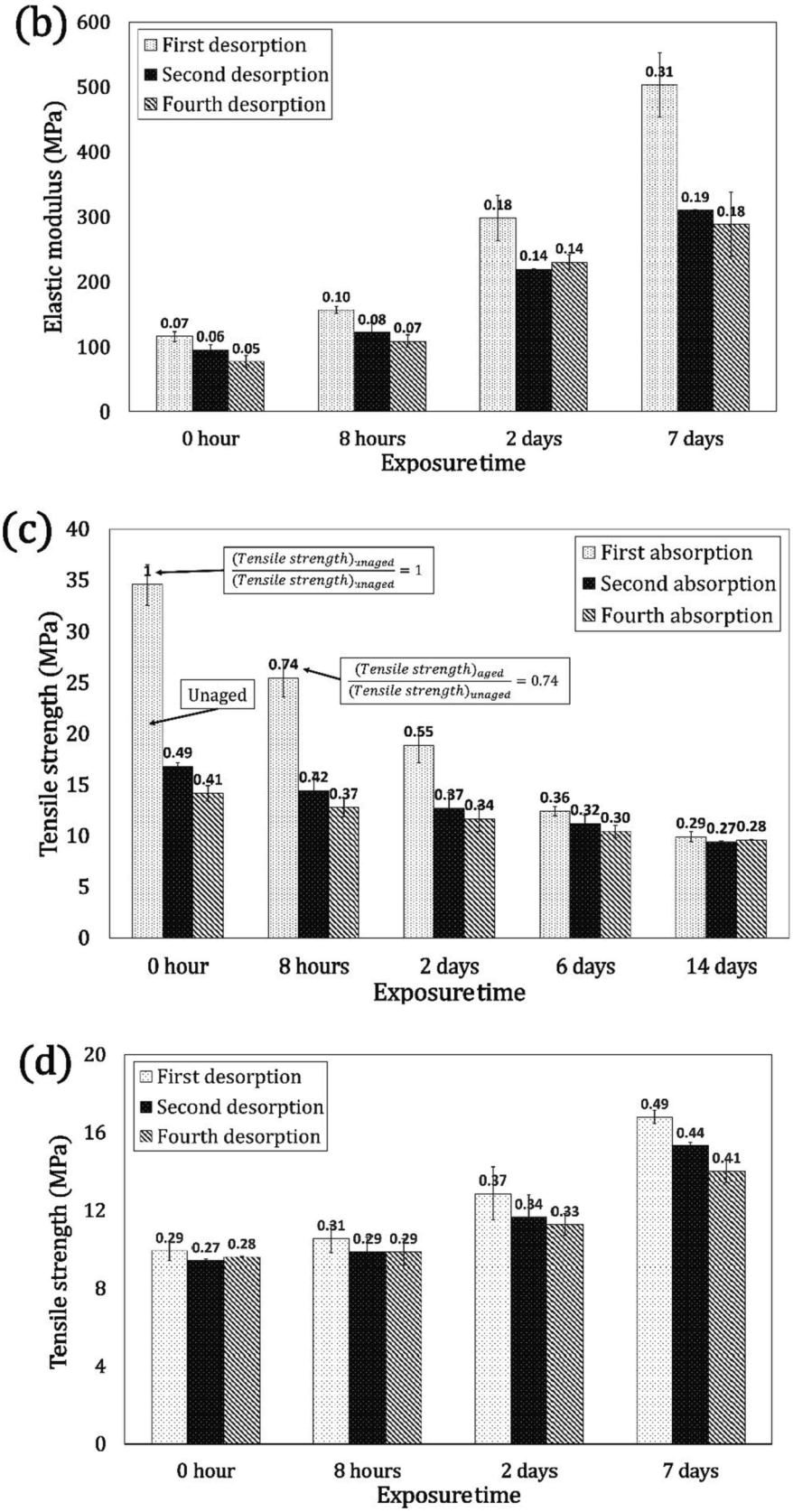

Fig. 12. (*continued*).

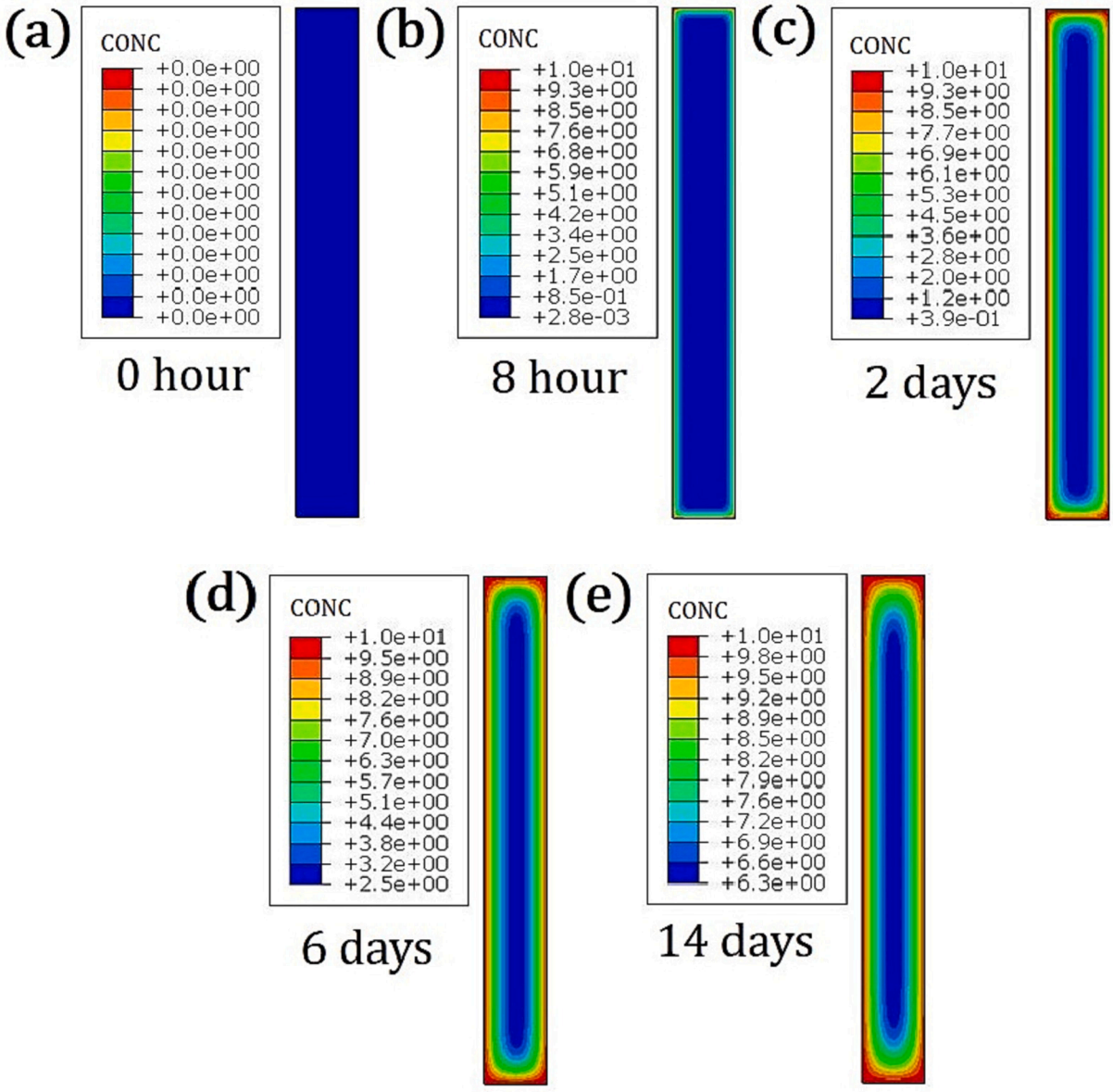

Fig. 13. Moisture distribution of dogbone cross-section for unaged (a) and after 8 h (b), and 2 (c), 6 (d), and 14 (e) days ageing for the first absorption cycle.

energy in mode II.

The numerical simulations in this study utilized 3D state of stress by considering C3D8R elements (8-node linear solid elements in Abaqus). The cohesive layer, was modelled with 8-node 3D cohesive elements (COH3D8). The configuration of the elastic and cohesive elements in DCB specimens is depicted in Fig. 8.

The cohesive elements were modelled as a single row in the middle of the adhesive layer with a thickness of 0.1 mm. The suitable dimension of cohesive elements was obtained based on mesh convergence analysis.

4. Results and discussions

4.1. Flexural properties of GFRP substrates

Previous researchers revealed that moisture diffusion can change the flexural modulus of GFRP laminates [30]. The variation of flexural modulus in GFRP substrate during the cyclic ageing changes mode mixity in dissimilar DCB adhesive joints [49]. As a result, the variation of the flexural modulus of GFRP substrates in different ageing cycles should be considered in numerical simulations. In this section, the flexural parameters variation of GFRP specimens exposed to cyclic ageing is reported. For this purpose, the flexural stress–strain curves of GFRP specimens before ageing and after the first, second, and fourth absorption process were measured using three points bending test. The flexural stress–strain curves of the unaged and aged GFRP specimens are represented in Fig. 9.

Based on curves obtained for the GFRP substrates, the flexural modulus and strength of GFRP in different ageing conditions were calculated. Fig. 10 shows the flexural modulus and strength of GFRP specimens after different ageing cycles.

Based on the results presented in Fig. 10, it can be inferred that the flexural modulus of GFRP substrates remains relatively constant during

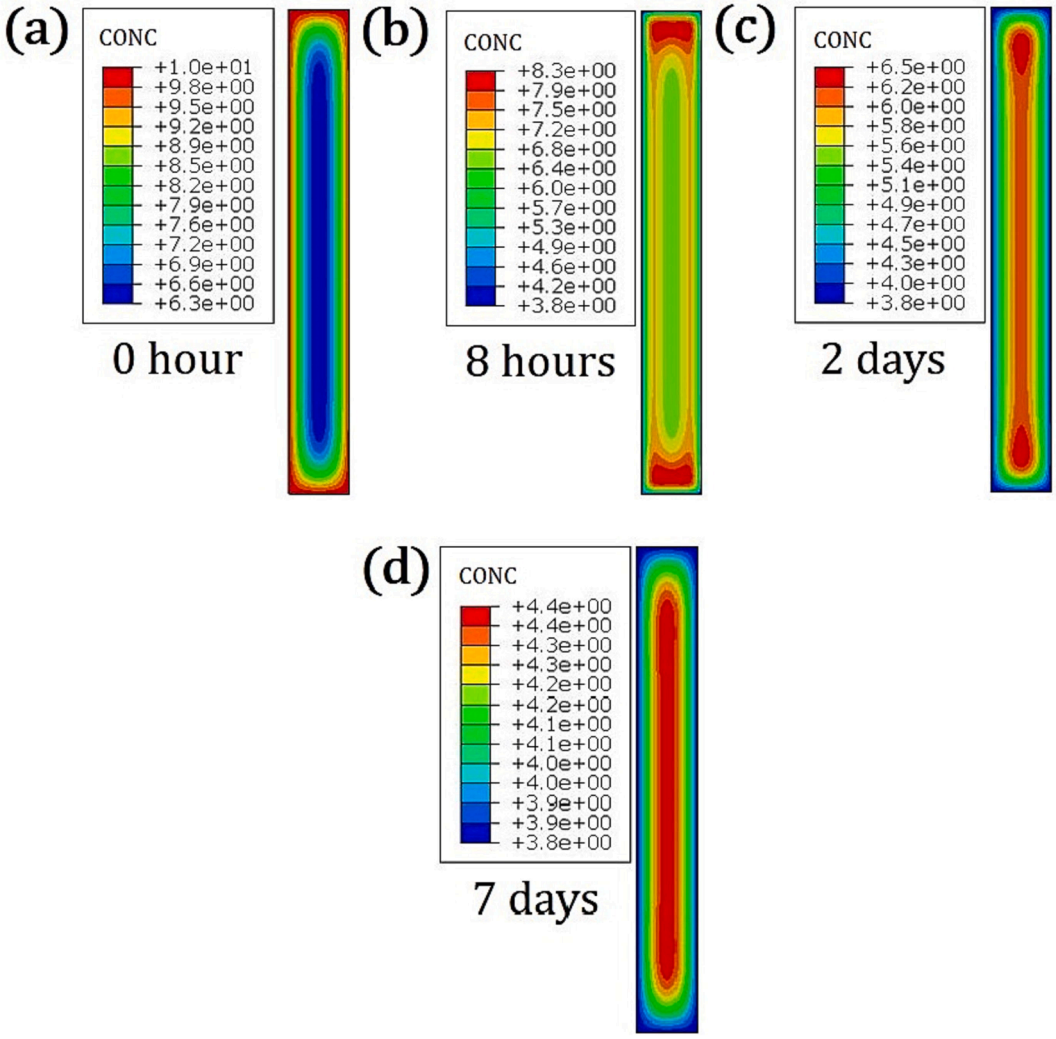

Fig. 14. Moisture distribution of dogbone cross-section for (a) unaged, (b) 8 h drying, (c) 2 days drying, and (d) 7 days drying for the first desorption process.

cyclic ageing, whereas the flexural strength experiences a substantial decrease after the first cycle, with further negligible changes. These findings indicate that the flexural modulus can be considered a reliable parameter for simulating DCB specimens during different ageing cycles, and has been utilized as such in this study.

4.2. Stress-strain curves of aged dogbone specimens

This section presents the stress–strain curves for dogbone specimens that were unaged and subjected to cyclic aging at varying levels of moisture content and cycles. The obtained stress–strain curves were used to determine the tensile strength and elastic modulus of the adhesive for different moisture exposure times and aging cycles. The tensile stress–strain curves for various exposure times and cycles are displayed in Fig. 11.

The stress–strain curves of unaged and cyclically aged dogbone specimens with different levels of moisture content and ageing cycles are presented in this section. Fig. 11 illustrates the tensile stress–strain curves after different moisture exposure times and ageing cycles. The results indicate that the tensile strength and elastic modulus of the adhesive decrease with increasing exposure time (Fig. 11a, c, and e). The reduction of these parameters is more prominent during the first moisture absorption process compared to subsequent cycles. During the moisture desorption process after different ageing cycles, the elastic modulus and tensile strength of the dogbone specimens increase (Fig. 11b, d, and f). Thus, the material becomes more ductile with moisture absorption and more brittle with moisture desorption. The comparison of stress–strain curves after different absorption and desorption cycles indicates that the tensile strength and elastic modulus vary significantly at the beginning of each process compared to long-term ageing results. Fig. 12 illustrates the influence of ageing conditions on the tensile strength and elastic modulus of the adhesives. To have a better perception of the variation of these parameters after different aging conditions, the ratio *aged/unaged* were also added to Fig. 12.

€As can be observed from Fig. 12, during the process of moisture absorption the tensile parameters of different ageing cycles tend to have similar values for higher exposure times (see Fig. 12a and c). In contrast, after the drying process, the difference between tensile parameters increases (see Fig. 12b and d).

In order to investigate the relationship between the mechanical properties of the adhesive and its moisture content and ageing cycles, a numerical simulation of the moisture distribution within the dogbone specimens was conducted at various exposure times. The simulation was based on the moisture diffusion parameters, including the diffusion constant and moisture contents, which were determined in a prior study. Fig. 5a illustrates the results of the moisture distribution simulation [22]. Details of the moisture distribution simulation process can be found in [17]. The moisture distribution in dogbone cross-section during the first cycle is shown in Figs. 13 and 14 as a function of exposure times.

The moisture content of dogbone specimens was calculated from the moisture distribution of specimen cross-section obtained from numerical simulation. For this purpose the average of moisture concentration in dogbone cross-section nodes obtained from FEM simulation were calculated in each exposure times and defined as moisture content parameter. Based on the results shown in Figs. 13 and 14, the moisture content in the first desorption process is more than 0 w%, due to the remaining moisture from the previous cycle. The results of previous investigations [22] show that numerical simulations of moisture distribution based on Fick's law constant for Araldite 2011 is a reliable technique for the calculation of the moisture level. Fig. 15 shows the effect of moisture content on the tensile strength and elastic modulus for different ageing cycles.

Fig. 15 depicts the variation of elastic modulus and tensile strength of the adhesive as a function of moisture content and ageing cycles. The results indicate that during the first moisture absorption process, both elastic modulus and tensile strength decrease substantially with increasing moisture content. However, during the subsequent moisture desorption process, as the moisture content decreases, tensile strength as well as the Young's modulus increase significantly. Nonetheless, these parameters do not fully recover to their unaged levels after the desorption process, and there is still a significant reduction in elastic modulus and tensile strength after the first cycle compared to the unaged condition. During the second and fourth cycles of moisture absorption and desorption, the elastic modulus and tensile strength decrease and increase gradually, respectively. Comparing the results during the second and fourth cycles reveals that their changes strongly depend on moisture content after the first cycle, while their sensitivity to ageing cycles is not significant.

4.3. Moisture distribution in DCB joints

In this section, the results of moisture distribution simulation in the DCB adhesive layer are reported. For this purpose, the adhesive layer between two substrates was simulated based on Fick's law constant and considering suitable boundary conditions (see Fig. 5b). Fig. 16 illustrates

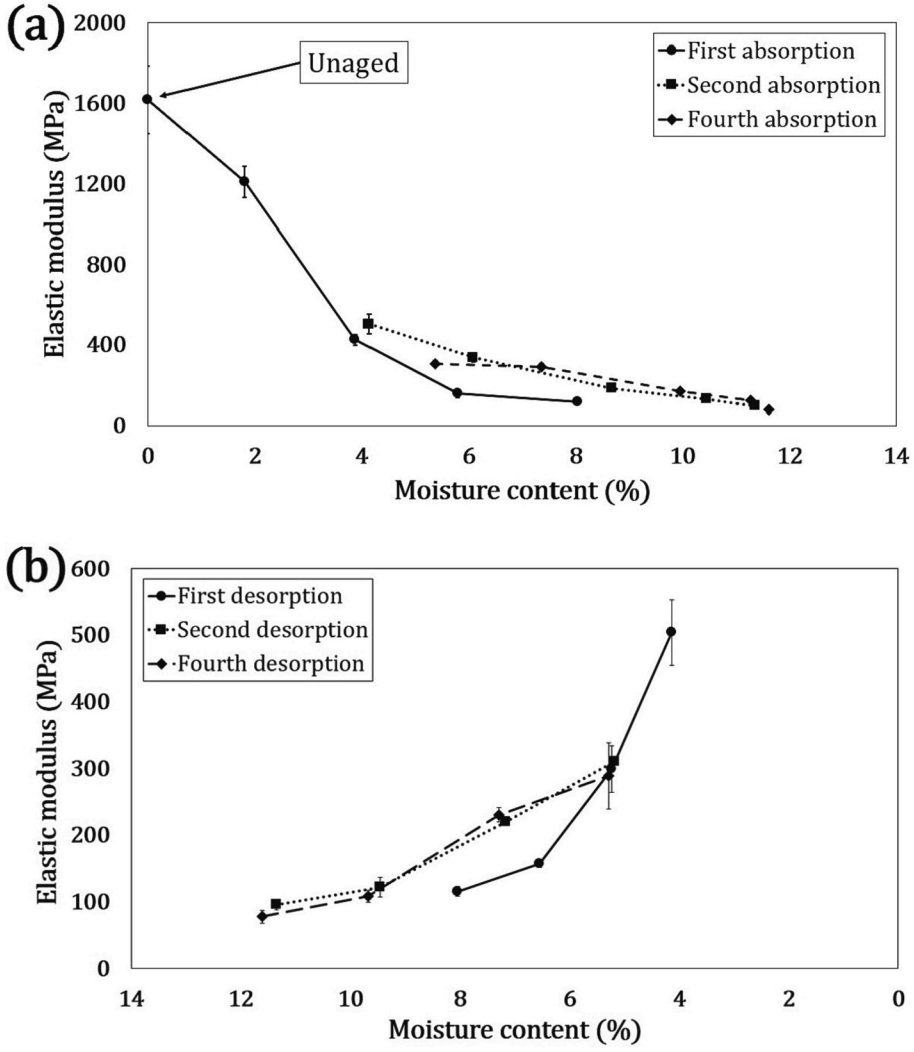

Fig. 15. Elastic modulus as a function of (a) absorption and (b) desorption process and also the effects of absorption (c) and desorption (d) on the tensile strength.

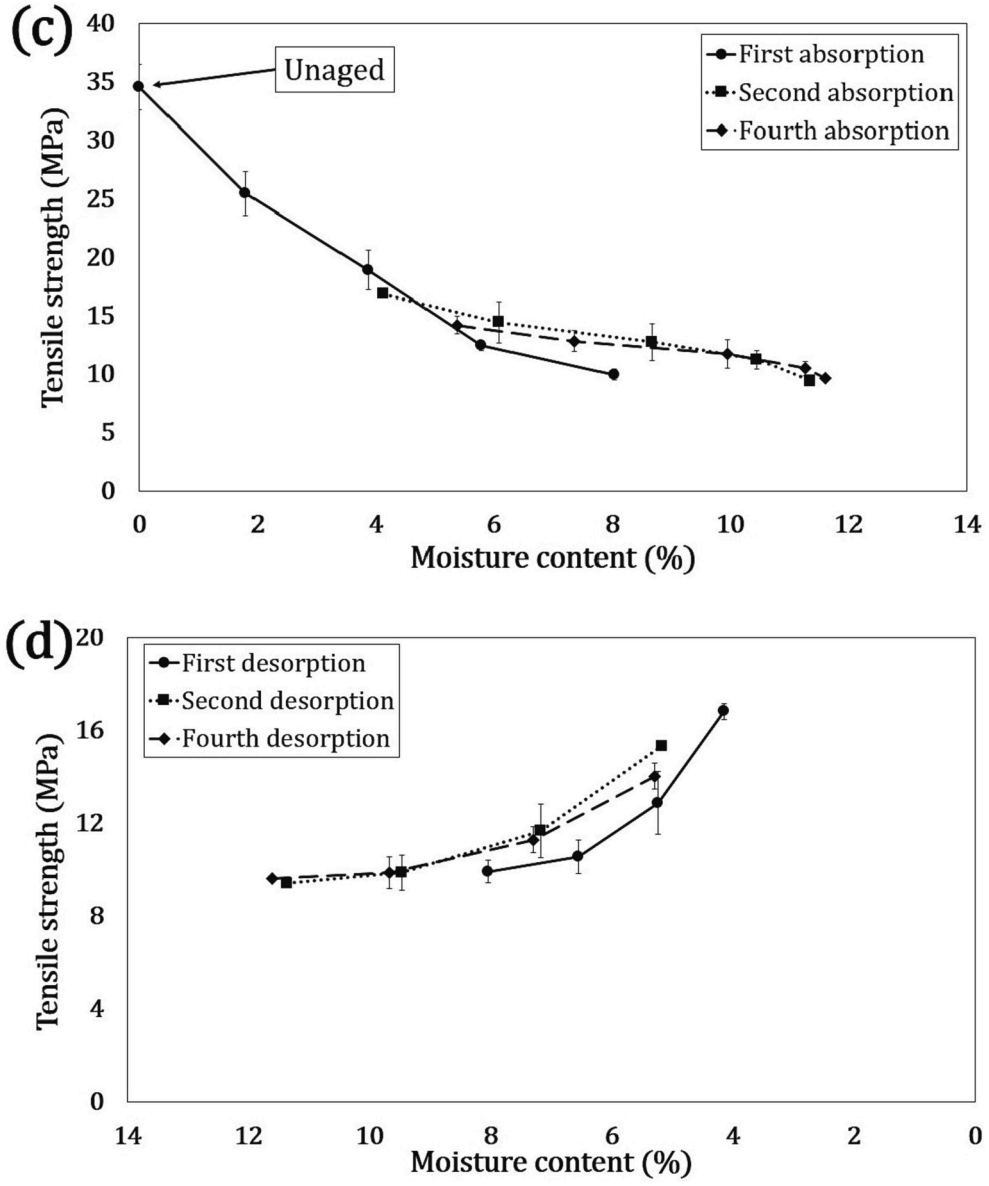

Fig. 15. (*continued*).

moisture concentration distribution in the adhesive layer at the end of different absorption and desorption process.

According to the results it is observed that the distribution of moisture in the adhesive is completely different from aged dogbone specimens (see Figs. 13 and 14). This difference is due to different boundary conditions. Accordingly, for simulation of aged DCB adhesive joints using CZM, the traction-separation curves should be defined as a function of the distribution of moisture through the bondline in DCBs.

4.4. Exposure time and cycle-dependent cohesive zone model

The aim of this study was to predict the load–displacement behavior of DCB adhesive joints under various ageing cycles using a degradable time-dependent traction-separation law. To accomplish this, cohesive parameters were varied based on experimental results and extrapolation techniques to reflect different ageing conditions. The triangular traction-separation curves, which are characterized by initial stiffness, maximum cohesive traction, and fracture energy, were generated using the variation of cohesive parameters during moisture absorption processes. For determination of these curves in different aging conditions, the variation of three parameters including: elastic modulus, tensile strength and fracture energy should be considered as a function of moisture content. Elastic modulus and tensile strength variations were determined from the tensile tests of dogbone specimens in different aging conditions, during this research. In addition, the variation of fracture energy in different moisture contents were reported using open DCB (ODCB) specimens in previous investigation [22]. It means that, in elastic modulus and tensile strength parameters the moisture distribution in dogbone specimen should be considered, but in fracture energy variation the moisture content of ODCB adhesive layer is important. Because of different geometries of adhesive layer and dogbone specimens the moisture distribution of dogbone and ODCB specimens in the same aging time are different. As a results, plotting of traction-separation curves as a function of moisture content needs some interpolation estimation. The resulting traction-separation curves for different moisture contents are presented in Fig. 17.

In these curves the moisture contents parameters are determined based on moisture distribution of dogbone specimens in different aging

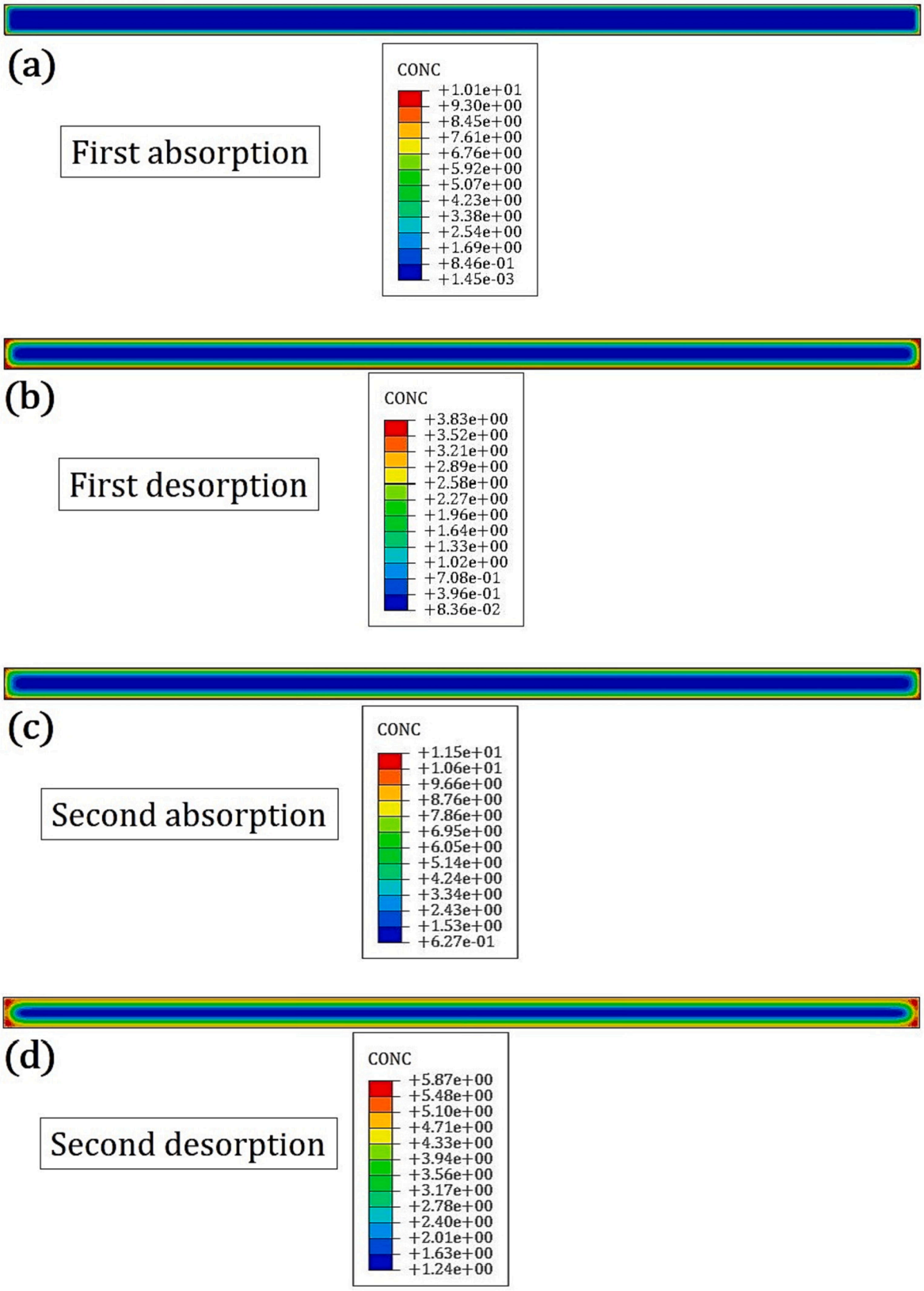

Fig. 16. Moisture distribution of DCB adhesive layer after the first absorption and desorption (a and b, respectively), second absorption and desorption (c and d, respectively) and fourth absorption and desorption (e and f respectively) (see Fig. 5b).

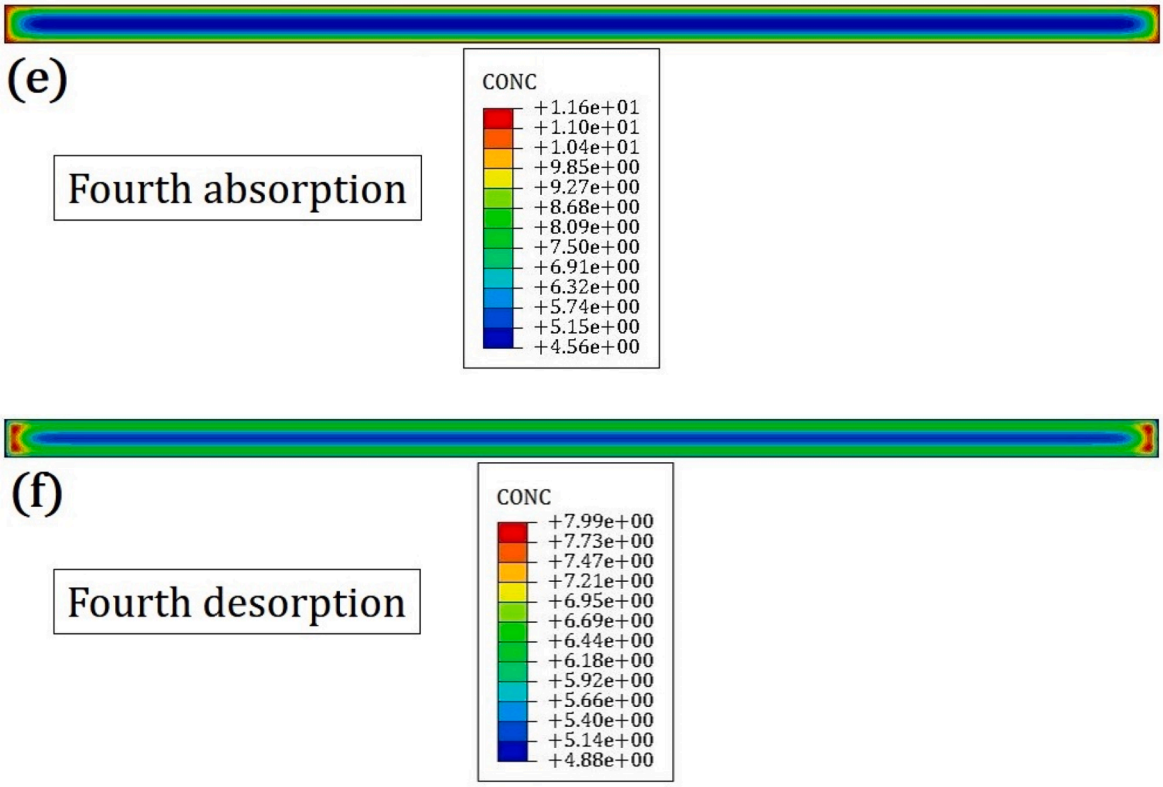

Fig. 16. (*continued*).

times and fracture energy parameters in calculated moisture content were estimated using interpolation process. For this purpose, after simulation of moisture distribution in specimen cross-section the average of moisture concentration in all FEM nodes was calculated and defined as moisture content parameters. The moisture concentration simulation in DCB adhesive layer (see Fig. 16) shows that moisture distributions in adhesive layer are different from that in dogbone specimens (see Fig. 14). As a results, the traction-separation curves in some moisture contents should be extrapolated based on the experimental results. In other words, the moisture contents in which traction-separation curves are illustrated as a function of moisture distribution in DCB adhesive layer (see Fig. 16).

As can be seen in Fig. 17, the initial stiffness and cohesive traction decrease and damage initiation separation and the critical effective separation value (separation with complete damage) increase a function of the ageing time at each cycle. Previous investigated results [22] show that fracture energy decreases with increasing moisture content.

4.5. CZM model validation

In order to validate the CZM, firstly, the crack propagation path of aged DCB specimens should be checked since the CZM model developed is valid only in cohesive failure condition. For this purpose, the fracture surface of all specimens were carefully analyzed by visual observation and in some selected samples using the Keyence VR 5000 wide-area 3D profiling system as shown in Fig. 18. Based on the roughness of the fracture surface and on the thickness of the substrate, the thickness of the remaining adhesive on the fractured surface was determined. For all of DCB specimens, the cohesive failure through the adhesive layer was confirmed.

To accurately predict the load–displacement curves of dissimilar DCB adhesive joints subjected to different ageing cycles, it is necessary to simulate the moisture distribution in the adhesive layer. This was achieved through numerical simulation of moisture diffusion constants and boundary conditions during different moisture absorption processes in the adhesive layer of the DCB specimen. The resulting moisture distribution was measured in each element of the adhesive layer during different ageing cycles (see Fig. 16). Subsequently, cohesive elements in the Abaqus software were applied with traction-separation curves based on their moisture contents using a user material routine (UMAT). Cohesive parameters for each element were defined based on experimental results obtained from the present and previous studies [22]. Fig. 19 shows the flowchart of FEM implementation.

The developed numerical model was then used to predict the load–displacement curves of DCB adhesive joints after the first, second, and fourth absorption cycles. To validate the developed numerical model, load–displacement curves for unaged dissimilar adhesive joints were simulated numerically and compared with experimental results. Fig. 20 demonstrates the comparison between experimental and numerical load–displacement curves for unaged DCB specimens.

The comparison of the obtained results from experimental tests and CZM shows that the developed CZM can estimate load–displacement curves of unaged dissimilar DCB adhesive joints precisely. Using the numerical model and based on cohesive parameters variation in different ageing conditions, the load–displacement curves of unaged and aged DCB adhesive joints after the first, second, and fourth absorption process were calculated numerically. Fig. 21 shows the variation of load–displacement curves in different moisture absorption processes.

The comparison of the load–displacement curves reveals that there is a slight decrease in the maximum load after the first absorption process,

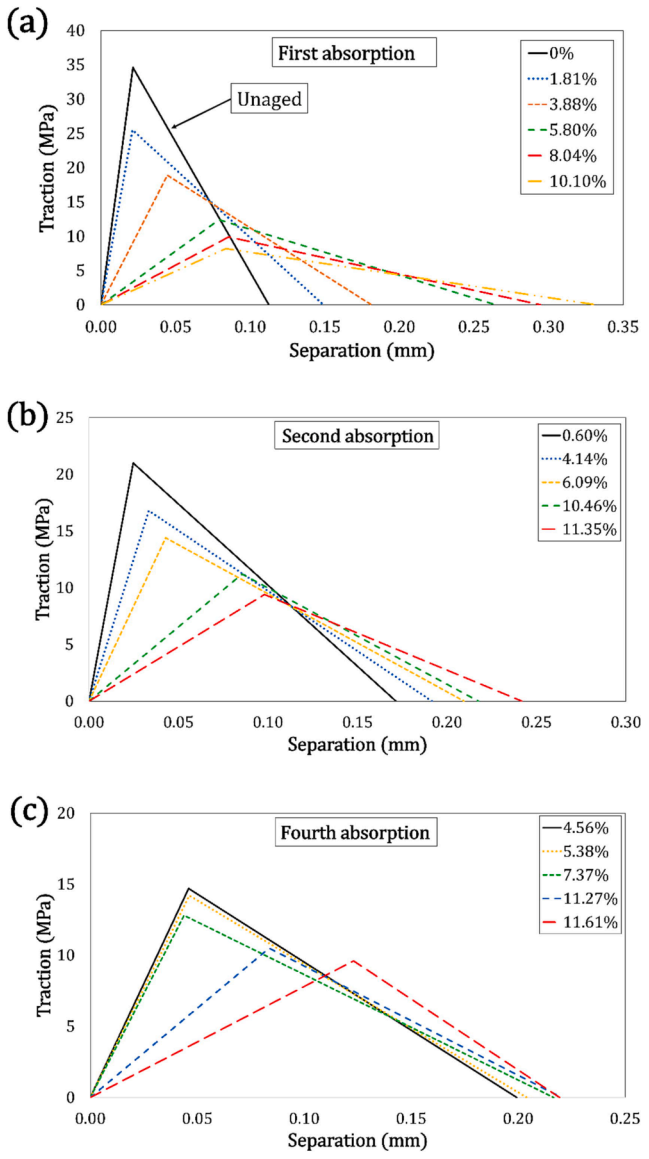

Fig. 17. Traction-separation laws as a function of moisture contetn and cycle: first cycle (a), second cycle (b) and fourth cycle(c) absorption processes.

which is attributed to the minor moisture absorption in the adhesive layer during this stage (as depicted in Fig. 16a). Subsequently, with an increase in the number of ageing cycles, the maximum load significantly decreases in comparison to the unaged results. To verify the CZM model's accuracy, it was utilized for aged DCB specimens having a non-uniform distribution of water uptake along the overlap. The CZM-predicted load–displacement curves were then compared against the experimental results. Fig. 22 illustrates both the experimental and numerical load–displacement curves for DCB adhesive joints after the fourth absorption process.

The comparison between the experimental and numerical load–displacement curves in Fig. 22 indicates a discrepancy in the maximum load, which could be due to errors in the extrapolation process or experimental testing. However, the overall trend of the curves is similar, demonstrating the potential of the developed CZM for predicting load–displacement curves in DCB specimens after cyclic ageing. In order to compare numerical and experimental results, the initial stiffness and maximum loads obtained from CZM and experiments are reported in Table 2.

The comparison of the maximum load and initial stiffness obtained from CZM and experiments for unaged and aged specimens after fourth absorption shows that the developed CZM can estimated load–displacement behaviour of DCB specimen with high accuracy.

5. Conclusions

This study explored the impact of cyclic ageing on the mechanical behavior of DCB adhesive joints featuring dissimilar substrates of GFRP and aluminum. To accomplish this, the study developed a mode I cohesive zone model that degrades with respect to both moisture content and ageing cycles. The following points can be drawn out of the results.

- The variation in the flexural modulus of GFRP substrates exposed to cyclic moisture absorption is negligible.
- During cyclic ageing, the tensile strength (and elastic modulus) of the adhesive decrease as a result of moisture absorption and increase during the desorption process.
- The effect of ageing cycles on the tensile strength and elastic modulus decreases with increasing number of cycles.
- The initial stiffness and cohesive traction decrease while the damage initiation separation and critical effective separation value increase with increasing moisture content.

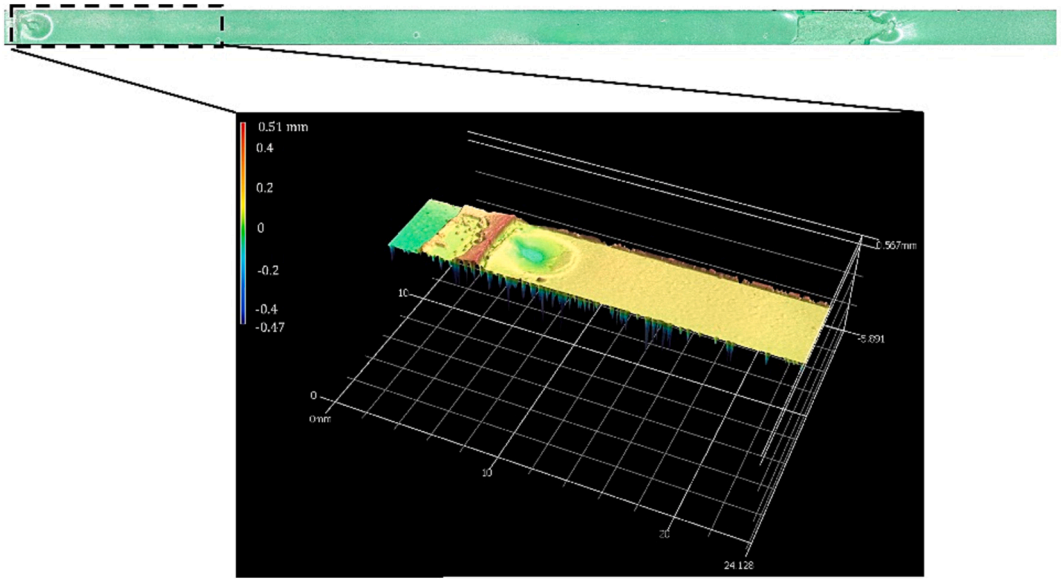

Fig. 18. A 3D scan of surface fracture near the crack tip.

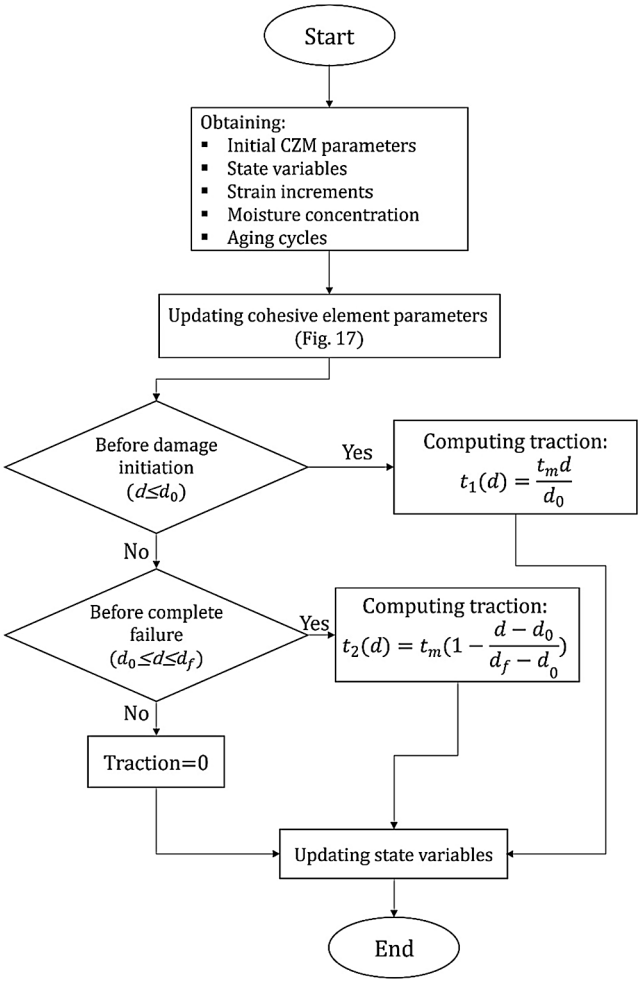

Fig. 19. Flowchart of FEM implementation.

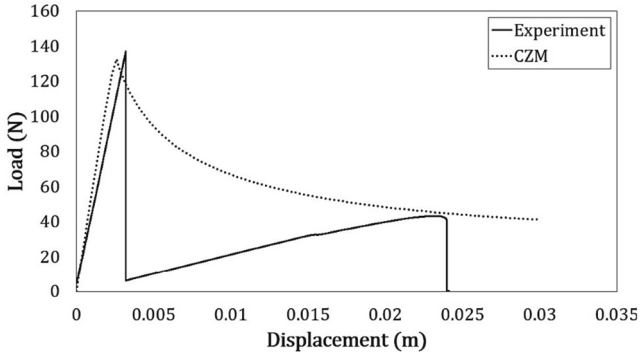

Fig. 20. Load-displacement curves for an unaged DCB specimen obtained experimentally and numerically.

- The use of CZM and user material routine in numerical simulation of dissimilar DCB adhesive joints has shown to be an accurate method for predicting the strength of cyclically aged adhesive joints.
- The load–displacement curves of DCB adhesive joints for unaged conditions and after the first absorption are similar, which could be due to the minimal moisture diffusion during the first absorption.
- A significant reduction in the DCB strength was found during the second and fourth moisture absorption cycles.

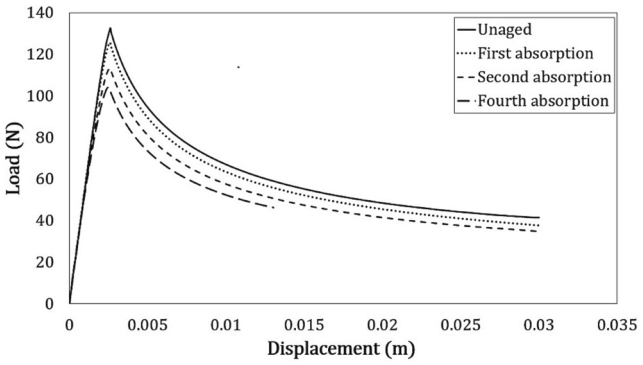

Fig. 21. Load-displacement curves for unaged and aged DCB specimens at the end of the moisture absorption process in different ageing cycles obtained numerically.

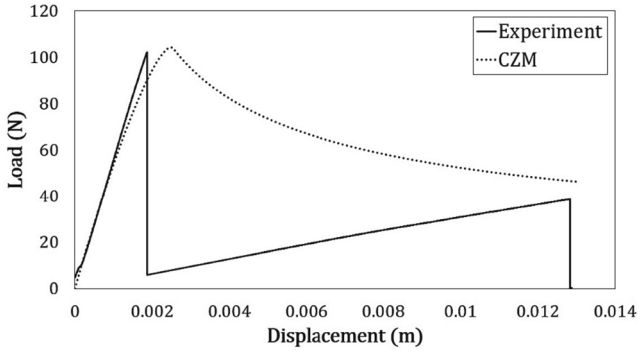

Fig. 22. Load-displacement curves for DCB specimen after fourth absorption obtained experimentally and numerically.

Table 2
Initial stiffness and maximum load obtained from experiments and CZM for unaged and aged specimens after fourth absorption.

Parameters	Unaged		Fourthabsorption	
	CZM	Experiments	CZM	Experiments
Initial stiffness (N/m)	54,200	49,091	49,000	50,400
Maximum load (N)	132.54	137.07	104.18	107.46

CRediT authorship contribution statement

M. Moazzami: Conceptualization, Methodology, Validation, Investigation, Data curation, Writing – original draft, Visualization. **A. Akhavan-Safar:** Conceptualization, Methodology, Writing – original draft, Writing – review & editing, Visualization. **M.R. Ayatollahi:** Conceptualization, Writing – review & editing, Visualization, Supervision. **J.A. Poulis:** Methodology, Investigation, Resources, Writing – review & editing, Visualization, Supervision. **L.F.M. da Silva:** Writing – review & editing, Visualization, Supervision. **S. Teixeira De Freitas:** Methodology, Investigation, Resources, Writing – review & editing, Visualization, Supervision.

Declaration of Competing Interest

The authors declare that they have no known competing financial interests or personal relationships that could have appeared to influence the work reported in this paper.

Data availability

Data will be made available on request.

References

[1] M.D. Banea, L.F. da Silva, R.D. Campilho, C. Sato, Smart adhesive joints: An overview of recent developments, J. Adhes. 90 (1) (2014) 16–40.
[2] A.P. Mouritz, E. Gellert, P. Burchill, K. Challis, Review of advanced composite structures for naval ships and submarines, Compos. Struct. 53 (1) (2001) 21–42.
[3] M.D. Banea, L.F. da Silva, Adhesively bonded joints in composite materials: an overview, Proc. Inst. Mech. Eng., Part L: J. Mater.: Design Appl. 223 (1) (2009) 1–18.
[4] S. Safaei, M. Ayatollahi, A. Akhavan-Safar, M. Moazzami, L. Da Silva, Effect of residual strains on the static strength of dissimilar single lap adhesive joints, J. Adhes. 97 (11) (2021) 1052–1071.
[5] W. Wang, S.T. De Freitas, J.A. Poulis, D. Zarouchas, A review of experimental and theoretical fracture characterization of bi-material bonded joints, Compos. B Eng. (2020), 108537.
[6] A. Akhavan-Safar, R. Beygi, F. Delzendehrooy, L. da Silva, Fracture energy assessment of adhesives–Part I: Is GIC an adhesive property? A neural network analysis, Proc. Inst. Mech. Eng., Part L: J. Mater.: Design Appl. 235 (6) (2021) 1461–1476.
[7] A. Akhavan-Safar, M. Ayatollahi, M. Moazzami, L. Da Silva, The role of T-stress and stress triaxiality combined with the geometry on tensile fracture energy of brittle adhesives, Int. J. Adhes. Adhes. 87 (2018) 12–21.
[8] W. Wang, R.L. Fernandes, S.T. De Freitas, D. Zarouchas, R. Benedictus, How pure mode I can be obtained in bi-material bonded DCB joints: a longitudinal strain-based criterion, Compos. B Eng. 153 (2018) 137–148.
[9] M. Moazzami, M. Ayatollahi, S.T. de Freitas, L. da Silva, Towards pure mode I loading in dissimilar adhesively bonded double cantilever beams, Int. J. Adhes. Adhes. 107 (2021), 102826.
[10] M. Khoshravan, F.A. Mehrabadi, Fracture analysis in adhesive composite material/aluminum joints under mode-I loading; experimental and numerical approaches, Int. J. Adhes. Adhes. 39 (2012) 8–14.
[11] D. Chalmers, The potential for the use of composite materials in marine structures, Mar. Struct. 7 (2–5) (1994) 441–456.
[12] J. Leplat, G. Stamoulis, P. Bidaud, D. Thevenet, Measurement of the interfacial strain energy release rate of adhesively bonded structures with metallic substrates before and after water ageing, Theor. Appl. Fract. Mech. 121 (2022), 103511.
[13] N. Omidvar, H. Khoramishad, M. Aliha, Investigation of the deleterious effects of low-temperature and hygrothermal aging conditions on the mixed-mode fracture resistance of epoxy resin using a short-beam bend specimen, Theor. Appl. Fract. Mech. 121 (2022), 103539.
[14] S. Abdel-Monsef, J. Renart, L. Carreras, A. Turon, P. Maimí, Effect of environment conditioning on mode II fracture behaviour of adhesively bonded joints, Theor. Appl. Fract. Mech. 112 (2021), 102912.
[15] Y. Hua, A. Crocombe, M. Wahab, I. Ashcroft, Modelling environmental degradation in EA9321-bonded joints using a progressive damage failure model, J. Adhes. 82 (2) (2006) 135–160.
[16] S. Sugiman, A. Crocombe, I. Aschroft, Experimental and numerical investigation of the static response of environmentally aged adhesively bonded joints, Int. J. Adhes. Adhes. 40 (2013) 224–237.
[17] M. Moazzami, M. Ayatollahi, A. Akhavan-Safar, L. Da Silva, Experimental and numerical analysis of cyclic aging in an epoxy-based adhesive, Polym. Test. 91 (2020), 106789.
[18] H. Khoramishad, O. Alizadeh, Effects of silicon carbide nanoparticles and multi-walled carbon nanotubes on water uptake and resultant mechanical properties degradation of polymer nanocomposites immersed in hot water, Polym. Compos. 39 (S2) (2018) E883–E890.
[19] J. Da Costa, A. Akhavan-Safar, E. Marques, R. Carbas, L. Da Silva, Cyclic ageing of adhesive materials, J. Adhes. (2021) 1–17.
[20] P. Fernandes, G. Viana, R. Carbas, M. Costa, L. Da Silva, M. Banea, The influence of water on the fracture envelope of an adhesive joint, Theor. Appl. Fract. Mech. 89 (2017) 1–15.
[21] T. A. Rodrigues, F. J. Chaves, L. F. d. Silva, M. Costa, and A. Q. Barbosa, "Determination of the fracture envelope of an adhesive joint as a function of moisture: Bestimmung der Bruchumgebung für das Versagen einer Klebeverbindung als Funktion der Feuchtigkeit," *Materialwissenschaft und Werkstofftechnik*, vol. 48, no. 11, pp. 1181-1190, 2017.
[22] M.R.A. Mostafa Moazzami, A. Akhavan-Safar, S.T.D. Freitas, J.A. Poulis, L.FM. da Silva, Effect of cyclic aging on mode I fracture energy of dissimilar metal/composite DCB adhesive joints, Eng. Fract. Mech. (2022).
[23] J. Leplat, G. Stamoulis, P. Bidaud, D. Thévenet, Investigation of the mode I fracture properties of adhesively bonded joints after water ageing, J. Adhes. 98 (1) (2022) 68–89.
[24] G. Zheng, et al., On failure mechanisms in CFRP/Al adhesive joints after hygrothermal aging degradation following by mechanical tests, Thin-Walled Struct. 158 (2021), 107184.
[25] A. Chateauminois, L. Vincent, B. Chabert, J. Soulier, Study of the interfacial degradation of a glass-epoxy composite during hygrothermal ageing using water diffusion measurements and dynamic mechanical thermal analysis, Polymer 35 (22) (1994) 4766–4774.
[26] W. Li, X. Shao, L. Li, G. Zheng, Effect of hygrothermal ageing on the mechanical performance of CFRP/AL single-lap joints, J. Adhes. (2021) 1–28.
[27] B. Boukhoulda, E. Adda-Bedia, K. Madani, The effect of fiber orientation angle in composite materials on moisture absorption and material degradation after hygrothermal ageing, Compos. Struct. 74 (4) (2006) 406–418.
[28] C. Wang, J. Wang, T. Su, Determination of Water Diffusion Coefficients and Dynamics in Adhesive/Carbon Fiber-Reinforced Phenolic Resin Composite Joints, J. Adhes. 83 (3) (2007) 255–265.
[29] X. Jiang, H. Kolstein, F. Bijlaard, X. Qiang, Effects of hygrothermal aging on glass-fibre reinforced polymer laminates and adhesive of FRP composite bridge: Moisture diffusion characteristics, Compos. Part A: Appl. Sci. Manuf. 57 (2014) 49–58.
[30] S. Eslami, F. Taheri-Behrooz, F. Taheri, Effects of aging temperature on moisture absorption of perforated GFRP, Adv. Mater. Sci. Eng. 2012 (2012).
[31] E. Pérez-Pacheco, J. Cauich-Cupul, A. Valadez-González, P. Herrera-Franco, Effect of moisture absorption on the mechanical behavior of carbon fiber/epoxy matrix composites, J. Mater. Sci. 48 (5) (2013) 1873–1882.
[32] D.A. Bond, Moisture diffusion in a fiber-reinforced composite: part I–non-Fickian transport and the effect of fiber spatial distribution, J. Compos. Mater. 39 (23) (2005) 2113–2141.
[33] J. da Costa, A. Akhavan-Safar, E. Marques, R. Carbas, L. da Silva, The influence of cyclic ageing on the fatigue performance of bonded joints, Int. J. Fatigue 161 (2022), 106939.
[34] C. Borges, et al., Influence of water and surfactant contamination on the mechanical and chemical properties of a silicone adhesive before and after curing, J. Adhes. (2022) 1–28.
[35] J.A. da Costa, A. Akhavan-Safar, E. Marques, R. Carbas, L. da Silva, Effects of ageing frequency on the interfacial failure and tensile properties of adhesively bonded Arcan joints exposed to cyclic ageing environments, Proc. Inst. Mech. Eng., Part E: J. Process Mech. Eng. (2022).
[36] J. Da Costa, A. Akhavan-Safar, E. Marques, R. Carbas, L. Da Silva, Effects of cyclic ageing on the tensile properties and diffusion coefficients of an epoxy-based adhesive, Proc. Inst. Mech. Eng., Part L: J. Mater.: Design Appl. 235 (6) (2021) 1451–1460.
[37] A. Mubashar, I.A. Ashcroft, G.W. Critchlow, A. Crocombe, Moisture absorption–desorption effects in adhesive joints, Int. J. Adhes. Adhes. 29 (8) (2009) 751–760.
[38] H. Khoramishad, H. Bayati, D. Kordzangeneh, The deleterious effect of cyclic hygrothermal aging on nanocomposite adhesives, J. Adhes. (2020) 1–19.
[39] R.L. Fernandes, S.T. de Freitas, M.K. Budzik, J.A. Poulis, R. Benedictus, Role of adherend material on the fracture of bi-material composite bonded joints, Compos. Struct. 252 (2020), 112643.
[40] M. Moazzami, M. Ayatollahi, A. Akhavan-Safar, S. Teixeira de Freitas, L.F. da Silva, Cyclic aging analysis of CFRP and GFRP composite laminates, J. Compos. Mater. (2023).
[41] M. Costa, et al., Effect of the size reduction on the bulk tensile and double cantilever beam specimens used in cohesive zone models, Proc. Inst. Mech. Eng., Part L: J. Mater.: Design Appl. 230 (5) (2016) 968–982.
[42] A. Turon, C.G. Davila, P.P. Camanho, J. Costa, An engineering solution for mesh size effects in the simulation of delamination using cohesive zone models, Eng. Fract. Mech. 74 (10) (2007) 1665–1682.
[43] R.D.S.G. Campilho, M. De Moura, A. Barreto, J. Morais, J. Domingues, Fracture behaviour of damaged wood beams repaired with an adhesively-bonded composite patch, Compos. A Appl. Sci. Manuf. 40 (6–7) (2009) 852–859.
[44] A. Akhavan-Safar, E. A. Marques, R. J. Carbas, and L. F. da Silva, "Numerical Simulation," in *Cohesive Zone Modelling for Fatigue Life Analysis of Adhesive Joints*: Springer, 2022, pp. 67-88.
[45] A. Akhavan-Safar, E. A. Marques, R. J. Carbas, and L. F. da Silva, "Cohesive Zone Modelling-CZM," in *Cohesive Zone Modelling for Fatigue Life Analysis of Adhesive Joints*: Springer, 2022, pp. 19-42.
[46] R.D. Campilho, M.D. Banea, A.M. Pinto, L.F. da Silva, A. De Jesus, Strength prediction of single-and double-lap joints by standard and extended finite element modelling, Int. J. Adhes. Adhes. 31 (5) (2011) 363–372.
[47] P. Feraren, H.M. Jensen, Cohesive zone modelling of interface fracture near flaws in adhesive joints, Eng. Fract. Mech. 71 (15) (2004) 2125–2142.
[48] S. Li, M. Thouless, A. Waas, J. Schroeder, P. Zavattieri, Mixed-mode cohesive-zone models for fracture of an adhesively bonded polymer–matrix composite, Eng. Fract. Mech. 73 (1) (2006) 64–78.
[49] M. Moazzami, M.R. Ayatollahi, A. Akhavan-Safar, S. Teixeira De Freitas, J. A. Poulis, L.F. da Silva, Influence of cyclic aging on adhesive mode mixity in dissimilar composite/metal double cantilever beam joints, Proc. Inst. Mech. Eng., Part L: J. Mater.: Design Appl. (2022).